High-pressure polymorphism in salicylamide

Post-print of a peer-reviewed article published by the Royal Society of Chemistry.
Published article available at: http://dx.doi.org/10.1039/B921288D

Cite as:
Johnstone, R. D. L., Lennie, A. R., Parker, S. F., Parsons, S., Pidcock, E., Richardson, P. R., Warren, J. E., & Wood, P. A. (2010). High-pressure polymorphism in salicylamide. *CrystEngComm*, 12(4), 1065-1078.

Manuscript received: 13/10/2009; Accepted: 11/12/2009; Article published: 20/01/2010

High-Pressure Polymorphism in Salicylamide**

Russell D. L. Johnstone,[1] Alistair R. Lennie,[2] Stewart F. Parker,[3] Simon Parsons,[1,*] Elna Pidcock,[4] Patricia R. Richardson,[1] John E. Warren[2] and Peter A. Wood[4]

[1]EaStCHEM, School of Chemistry, Joseph Black Building, University of Edinburgh, West Mains Road, Edinburgh, EH9 3JJ, UK.

[2]Synchrotron Radiation Source, STFC Daresbury Laboratory, Warrington, Cheshire, WA4 4AD, UK.

[3]ISIS Pulsed Neutron and Muon Facility, STFC Rutherford Appleton Laboratory, Harwell Science and Innovation Campus, Chilton, Didcot, OX11 0QX, UK.

[4]Cambridge Crystallographic Data Centre, 12 Union Road, Cambridge, CB2 1EZ, UK.

[*]Corresponding author; e-mail: s.parsons@ed.ac.uk, fax: +44-(0)131 650 4743

[**]We thank the Cambridge Crystallographic Data Centre and the EPSRC for funding, and the STFC for provision of synchrotron and INS beamtime. We also thank the EaStCHEM Research Computing Facility for access to software and computing facilities. Finally, we thank Dr Stephen Moggach and Mr Alessandro Prescimone for their help with the synchrotron experiments.

Supporting information:
Electronic supplementary information (ESI) available: Quicktime movie showing the compression of salicylamide-I when viewed along the b-axis. CCDC reference numbers 751100–751105. For ESI and crystallographic data in CIF or other electronic format see http://dx.doi.org/10.1039/B921288D

Graphical abstract:

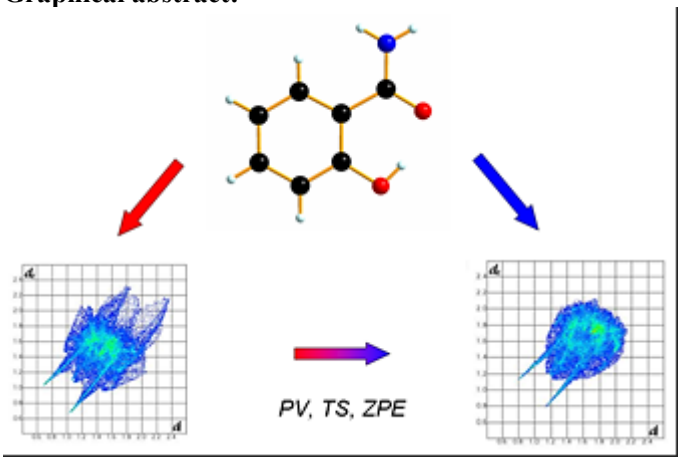

Synopsis:
The polymorph of salicylamide which is formed by crystal growth from solution at ambient pressure can be compressed to 5 GPa. Crystal growth *in situ* at 0.2 GPa yields a different polymorph where efficient H-bonding is sacrificed in favour of dispersion-dominated π..π and CH…π interactions. At 0.2 GPa the new polymorph is also stabilized by zero point energy and entropy effects.

Abstract

We report the compression of a single crystal of salicylamide to 5.1 GPa. Between ambient pressure and 5.1 GPa the structure remains in a compressed form of the ambient-pressure phase, referred as salicylamide-I. This phase has been investigated twice previously, but the coordinates appear to have been reported with respect to a non-standard space group origin, though no comment to this effect is made in either of the original reports. Short H…H contacts implied by the previously-published coordinates are strongly destabilizing according to PIXEL packing energy calculations, but are absent in the structure reported here. A new high-pressure polymorph, salicylamide-II, is formed if salicylamide is crystallized *in situ* from a saturated solution in a 4:1 mixture of methanol and ethanol at 0.2 GPa. Crystal growth yielded three crystallites within the pressure cell, and combination of single-crystal X-ray diffraction intensity data from all three yielded a data-set which was >90% complete. PIXEL calculations indicate that salicylamide-II exhibits weaker H-bonding but stronger dispersion interactions than phase-I. Harmonic frequencies calculated using periodic DFT (and validated by inelastic neutron scattering data) indicate that phase-II is favoured at high pressure by its lower volume, its lower zero point energy and higher entropy, and we estimate that at 0.2 GPa the free energy of phase-II is lower than that of phase-I by about 3 kJmol^{-1}.

Introduction

Understanding and prediction of polymorphism in the organic solid state is one of Chemistry's 'big questions'. Different polymorphs differ in solubility, ease of processing and reproducibility of formation. These properties are of particular importance to the pharmaceutical industry, which spends many millions of pounds each year on investigations of polymorphism of drug compounds, and our big question is one of real practical and commercial importance. Understanding why a polymorph forms under certain conditions but not under others forms an important component to work in the areas of polymorphism and crystal engineering.

Over the past ten years high pressure[1] has been shown to be a powerful tool for studying polymorphism. Numerous new high-pressure polymorphs have been generated for simple molecules such as alcohols and carboxylic acids,[1-4] for more complex systems, such as amino acids,[5] and for substantially larger systems such as energetic materials, pharmaceuticals,[6] metal-organic frameworks[7] and transition metal complexes.[8, 9] Over the course of our work in this area we have tried to understand the thermodynamic driving forces for pressure-induced phase transitions. In salicylaldoxime, for example, a transition between one form and another occurs at *ca.* 5 GPa, which we have shown relieves the strain generated in hydrogen bonds and π-π stacking interactions which are driven into repulsive regions of their potentials.[10]

In this paper we describe a study on the effect of pressure on salicylamide (Scheme I), a compound closely related to salicylaldoxime, the two being related by replacement of an oxime group by an amide. We show that although a new polymorph of salicylamide can be formed by *in situ* crystal growth from solution at 0.2 GPa, compression of the known ambient-pressure form does not result in any phase transformations, even up to 5 GPa. This result illustrates the need for the existence of an energetically accessible pathway for a phase transition to occur in a solid,[11] a feature also seen in compression studies of glycine, where different starting polymorphs yield different high-pressure forms.[12]

[1] The unit of pressure used in this paper is the gigapascal (GPa). 1 atm = 1.01325 × 10^{-4} GPa. 1 GPa = 10 kbar ~ 10 000 atm. Pressures at the bottom of deep sea trenches reach around 1000 atm ~ 1 kbar = 0.1 GPa.

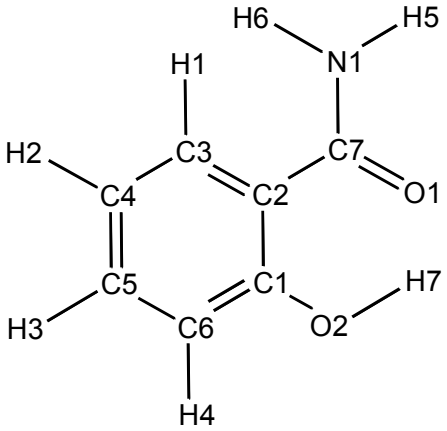

Scheme 1. Chemical structure diagram showing atomic numbering scheme of salicylamide.

When new polymorphs are generated by application of pressure, packing energy calculations can track the effects of compression on individual intermolecular interactions, revealing which interactions become repulsive, and which of these are relieved after a phase transition. When a new form crystallises directly from solution this conceptually simple means for understanding why polymorphism occurs is not available, and in this paper we attempt to address the features that make the new high-pressure polymorph of salicylamide thermodynamically competitive with the known form.

Experimental

The effect of pressure on salicylamide was investigated in two separate experiments. In one case pressure was applied to a crystal grown at ambient pressure. In the second experiment, a crystal was grown *in situ* at high pressure.

Salicylamide (99% purity, Scheme 1) was purchased from Aldrich (catalogue number 860417). A sample (0.5103 g) was dissolved in a 4:1 by volume mixture of methanol and ethanol (5 ml) and recrystallised by slow evaporation of the solvent. The solvent system used here is commonly used as a hydrostatic medium in high-pressure crystallography.

For one set of experiments a small, colourless, block-shaped crystal was loaded into a diamond anvil cell and used to study the effect of pressure on a single crystal grown *ex situ*. For the second set of experiments, a sample of the mother liquor from the same crystal growth experiment as described above was loaded into a separate diamond anvil cell and used for *in situ* crystal growth at high pressure (0.2 GPa). Crystal growth is described below.

Determination of the crystal structure of salicylamide under ambient conditions

In order to facilitate a comparison between ambient and high-pressure structures, diffraction data were also collected on salicylamide at ambient temperature and pressure. The crystal used was taken from the same batch as the sample used for the compression study. Data were measured on a Bruker SMART APEX diffractometer with graphite-monochromated Mo-Kα radiation (λ = 0.71073 Å) at room temperature. The data were integrated to $2\theta = 60°$ using SAINT[13] and corrected for absorption with SADABS.[14] The structure was solved using the program SIR-92[15] and structure refinement against $|F|^2$ using all data in CRYSTALS[16] yielded a conventional *R*-factor of 0.075. Crystal and refinement data are given in Table 1.

Pressure/ GPa	Ambient	0.3	2.0	4.0	5.1	0.2
Phase	I	I	I	I	I	II
Cell setting, space group	Monoclinic, *I*2/*a*	Monoclinic, *I*2/*a*	Monoclinic, *I*2/*a*	Monoclinic, *I*2/*a*	Monoclinic, *I*2/*a*	Orthorhombic, $P2_12_12_1$
a, b, c (Å)	12.8887 (8), 4.9700 (3), 20.9607 (19)	12.7925 (11), 4.9356 (5), 20.415 (5)	12.5438 (6), 4.8464 (3), 19.203 (3)	12.3706 (7), 4.7918 (3), 18.398 (3)	12.2791 (7), 4.7643 (3), 17.9649 (17)	3.8938 (4), 5.5612 (6), 28.566 (8)
α, β, γ (˚)	90, 91.546 (4), 90	90, 92.266 (14), 90	90, 93.648 (7), 90	90, 94.078 (8), 90	90, 93.960 (4), 90	90, 90, 90
V (Å)	1342.19 (17)	1288.0 (4)	1165.0 (2)	1087.8 (2)	1048.46 (13)	618.6 (2)
Z	8	8	8	8	8	4
D_x (Mg m^{-3})	1.357	1.414	1.564	1.675	1.737	1.472
μ (mm^{-1})	0.10	0.11	0.12	0.13	0.13	0.11
Crystal form, colour	Block, colourless	Block, colourless	Block, colourless	Block, colourless	Block, colourless	Block, colourless
Crystal size (mm)	0.57 x 0.36 x 0.32	0.20 x 0.20 x 0.10	0.20 x 0.20 x 0.10	0.20 x 0.20 x 0.10	0.20 x 0.20 x 0.10	Three crystallites, each 0.20 x 0.07 x 0.04
T_{min}	0.82	0.86	0.86	0.84	0.79	0.74
T_{max}	0.97	0.99	0.99	0.99	0.99	0.99
No. of measured, independent and observed reflections.	9399, 1778, 1434	4875, 814, 520	4594, 753, 564	4172, 721, 542	3937, 695, 566	10956, 720, 434
R_{int}	0.037	0.084	0.062	0.058	0.059	0.149
d_{max}, d_{min}/ Å	10.4, 0.72	4.6, 0.70	4.52, 0.70	4.46, 0.70	4.44, 0.70	5.46, 0.8
$R[F^2 > 2\sigma(F^2)]$, $wR(F^2)$, *S*	0.075, 0.138, 1.10	0.054, 0.128, 0.99	0.047, 0.111, 1.00	0.050, 0.119, 1.00	0.048, 0.124, 1.05	0.049, 0.126, 1.05
No. of parameters	95	95	95	95	95	95
$\Delta\rho_{max}$, $\Delta\rho_{min}$ (e Å^{-3})	0.34, -0.31	0.37, -0.36	0.27, -0.23	0.31, -0.31	0.27 -0.27	0.27, -0.30
Completeness to 0.8 Å	100%	45.7%	46.7%	46.5%	47.9%	90.9%

Table 1. Crystallographic data for salicylamide. In each case the formula is $C_7H_7NO_2$ and M_r = 137.14.

The results of the ambient pressure data collection showed the sample to have the same unit cell parameters and space group as those determined by Sasada *et al.*[17] and Pertlik.[18] Direct refinement of Pertlik's coordinates against our data set yielded a very high *R*-factor (0.51). The solution we present here differs from those given in references [17] and [18] by an origin-shift of [¼,-¼ ,¼]. We discuss the implication of this on crystal packing below.

High-Pressure Crystallography: Compression of a Single Crystal

High-pressure experiments were carried-out using a locally constructed Merrill-Bassett diamond anvil cell (half-opening angle 40°), equipped with Boehler–Almax cut diamonds with 600 μm culets and a tungsten gasket.[19, 20] A 1:1 mixture of *n*-pentane and isopentane was used as a hydrostatic medium, the purpose of which is to ensure that pressure is applied uniformly to the sample rather than along one direction. This hydrostatic medium is very volatile, and the cell was cooled in dry ice prior to loading. A small ruby chip was also loaded into the cell and the ruby fluorescence method used to measure the pressure.[21]

Diffraction data were collected on a Bruker-Nonius APEX-II diffractometer with silicon-monochromated synchrotron radiation (λ = 0.47540 Å) on Station 9.8 at the SRS, Daresbury Laboratory. Data collection and processing procedures for the high-pressure experiments followed Dawson *et al*.[22] Integrations were carried-out using dynamic masking of the regions of the detector shaded by the pressure cell[23] with the program SAINT. An absorption correction was carried-out in a two-stage procedure with the programs SHADE[24] and SADABS. Data were merged using SORTAV.[25, 26]

Data collections were taken at regular intervals from ambient pressure up to a final pressure of 5.1 GPa. The sample remained in a compressed form of phase-I (see Table 1). A further increase in pressure resulted in a marked broadening of the diffraction profiles, and no attempt was made to collect data at higher pressures.

Refinements of the compressed form of salicylamide-I were carried-out using the starting coordinates determined at ambient pressure and were refined against $|F|^2$ using all data in CRYSTALS. Owing to the low completeness of the data sets (Table 1), global rigid bond and body restraints were applied to the anisotropic displacement parameters. Restraints were also applied to all non-hydrogen primary intramolecular bond distances and angles based on the ambient pressure values.

Hydrogen atoms attached to carbon and nitrogen were placed geometrically and positions were not refined, isotropic displacement parameters were respectively set to 1.2 and 1.5 times those of the C or N host atoms. Hydrogens attached to oxygen atoms were located in Fourier difference maps and their positions were refined subject to an O-H distance restraint of 0.84(1) Å. A planarity restraint was applied to atoms H7, O2, C1, C2, C7 and O1. Since the orientation of the OH group is the only H-atom structural parameter not fixed by the geometry of the rest of the molecule an isotropic displacement parameter for H7 was refined independently with a restraint based on the ambient pressure value.

Compression of Salicylamide as Studied by Raman Spectroscopy

For the purposes of Raman spectroscopic measurements a single crystal of salicylamide-I was loaded into a Merrill-Bassett cell in the manner described above. Raman measurements were carried-out as a function of pressure by excitation with a 632.417 nm line from a He-Ne laser, the fluorescence being detected with a Jobin-Yvon LabRam 300 Raman spectrometer.

High-Pressure Recrystallisation

High-pressure recrystallisation of salicylamide from solution was performed using a Merrill-Basset diamond cell (half opening angle 40˚), equipped with brilliant-cut diamonds with 600 μm culets, a tungsten gasket and beryllium backing plates. At 0.2 GPa polycrystalline material precipitated. This was then almost completely redissolved with a heat gun, leaving a small seed crystallite. Slow cooling to room temperature produced three colourless crystals, each differently orientated inside the gasket hole. Diffraction data were collected using synchrotron radiation in the same manner as described above for the compression study. Determination of the cell dimensions showed the formation of a new polymorph of salicylamide (salicylamide-II) in space group $P2_12_12_1$ (Table 1).

The three domains were indexed and integrated separately, and then scaled and merged together in the program SORTAV[25, 26] to yield a data set of better than 90% completeness. The structure was solved using the program SIR-97.[27] Refinement was carried-out against $|F|^2$ using all data (CRYSTALS) from all three domains to give a conventional *R*-factor of 0.049. All non-H atoms were refined with anisotropic displacement parameters. Hydrogen atom treatment was the same as for high-pressure structures of salicylamide-I.

Release of pressure from the cell caused the crystal to redissolve, and we were not able to recover it at ambient conditions.

DFT Calculations

Periodic density functional theory (DFT) calculations were carried-out using the DMOL^3 code[28] as incorporated in the Materials Studio suite of software.[29] The PW91 GGA exchange-correlation functional[30] was used with the DND basis set. DND is a numerical basis set which includes polarizing d-functions on all non-H atoms; it is thought to provide reasonable accuracy at modest computational cost.

The *k*-point sampling was 4 × 4 × 2 with a grid size of 0.05 Å^{-1}; the optimisation energy convergence criterion was $\Delta E_{opt} < 2 \times 10^{-5}$ Hartree. The coordinates of the atoms in the solid state structure were allowed to optimise, while keeping the unit cell dimensions fixed. Following geometry optimisation vibrational frequencies were calculated at the Γ-point in the harmonic approximation. With the exception of three zero-frequency modes corresponding to acoustic phonons, all frequencies were positive. The structures studied in this way were salicylamide-I at ambient pressure and 0.3 GPa and salicylamide-II at 0.2 GPa.

Inelastic Neutron Scattering

Inelastic neutron scattering (INS) data were collected on the TOSCA instrument[31] at the ISIS neutron spallation facility. A polycrystalline sample of salicylamide-h_7 (3.2243 g) was used as obtained from Aldrich. The spectra were recorded using a flat sample can at 20 K. INS data were visualised and compared to the results of the DFT calculations using the ACLIMAX program.[32]

PIXEL Calculations

The final crystal structures obtained were used to calculate the molecular electron densities of the salicylamide molecules at each pressure by standard quantum chemical methods using the program GAUSSIAN03[33] with the MP2/6-31G** basis set. H-atom distances were set to standard neutron values in all calculations (C-H = 1.083 Å, N-H = 1.009 Å, O-H = 0.983 Å). The electron density was used to evaluate packing energies using the PIXEL method as implemented in the program OPiX.[34] The output from these calculations yields a total packing energy and a breakdown into component interactions. Each energy is further broken down into its Coulombic (electrostatic), polarisation, dispersion and repulsion contributions.[35, 36]

Hirshfeld Surface Calculations

Hirshfeld surface calculations were carried-out using CrystalExplorer.[37, 38] The wavefunction for electrostatic potential mapping was obtained at the HF/6-31G* level of theory using the TONTO package embedded in CrystalExplorer. The electrostatic potential was mapped between -0.04 (red, indicating regions of negative charge) and +0.04 (blue, for positively charged regions).

Other Programs Used

Crystal structures were visualised using the programs CAMERON[39], MERCURY 2.2[40] and DIAMOND.[41] Movies showing compression of the structures were made using CrystalMaker.[42] Analyses were carried-out using PLATON,[43] as incorporated in the WIN-GX suite.[44] Searches of the Cambridge Structural Database[45] utilized the program CONQUEST with database updates up to November 2008. Calculation of strain tensors were carried-out using a locally-written program[46] using the method described in Hazen & Finger.[47] Eigenvalues and vectors were calculated using the JACOBI routine in ref. [48].

Results

Salicylamide-I at ambient conditions

Salicylamide crystallises at ambient conditions with one molecule in the asymmetric unit in the space group *I*2/*a*. Each molecule is effectively planar: a least-squares mean plane calculated using all non-hydrogen atoms shows that the average deviation of these atoms from the plane is 0.014 Å.

PIXEL Interaction number	Interaction type	0 GPa	0.3 GPa	2.0 GPa	4.0 Gpa	5.1 GPa
Intramolecular interactions						
-	**O2H7...O1**[i] H7…O1 O2…O1 <O2H7O1	 1.71(3) 2.514(2) 156(3)	 1.72(2) 2.509(3) 154(2)	 1.69(2) 2.489(3) 155(2)	 1.69(3) 2.475(3) 155(3)	 1.68(3) 2.467(3) 153(3)
Network-building interactions						
#1	**N1H5...O1**[ii] H5…O1 N1…O1 <N1H5O1 Energy	 2.05 2.923(3) 175 -55.7	 2.02 2.898(4) 176 -56.3	 1.95 2.832(3) 177 -56.8	 1.90 2.782(3) 178 -53.4	 1.88 2.758(3) 177 -52.1
#2	**N1H6...O2**[iii] H6…O2 N1…O2 <N1H6O2 Energy	 2.14 3.000(2) 164 -33.0	 2.10 2.956(3) 164 -33.5	 1.99 2.841(2) 164 -32.5	 1.91 2.773(14) 165 -28.7	 1.88 2.735(2) 165 -25.5
Network-network interactions						
#3	**π...πi**[iv] Plane-plane Offset Energy	 3.203 6.551 -23.6	 3.149 6.519 -23.9	 2.967 6.458 -21.8	 2.828 6.396 -17.8	 2.750 6.347 -15.6
#6	**π...π**[vii] Plane-plane Offset Energy	 3.368 3.655 -7.2	 3.260 3.706 -6.9	 3.050 3.766 -1.4	 2.927 3.794 3.4	 2.859 3.811 8.1
Slab-slab interactions						
#4	**π...πi**[v] Plane-plane Offset Energy	 2.680 5.094 -10.3	 2.642 4.976 -11.1	 2.580 4.689 -12.3	 2.566 4.473 -11.2	 2.556 4.352 -10.3
#5	**C4H2...π**[vi] H2...π C4...π <C4H2π Energy	 3.23 4.035(3) 143 -10.0	 3.11 3.902(4) 143 -10.5	 2.83 3.626(4) 142 -10.0	 2.67 3.473(5) 143 -7.5	 2.61 3.411(3) 143 -6.2

Symmetry Operators:

i	*x,y,z*	v	1/2-*x,* -1/2-*y,* 3/2-*z*
ii	1- *x,*1-*y,*1-*z*	vi	1-*x*, -1/2+*y*, 3/2-*z*
iii	1/2+*x,*-*y,z*	vii	*x, y*-1, *z*
iv	1-*x, -y,* 1-*z*		

Table 2. Geometry of intermolecular interactions in salicylamide-I. Distances are in Å, and angles in °. Standard uncertainties were calculated in PLATON. Total interaction energies are also included from PIXEL calculations and are given in kJmol^{-1}. For CH…π interactions, distances and angles are measured with respect to the centroid of the rings.

Structure and Pressure	Interaction no. (see text)	Coulombic	Polarisation	Dispersion	Repulsion	Total	Symmetry operators
CSD Refcode SALMID01[18] (Ambient pressure)	-	-74.9	-24.9	-15.5	62.0	-53.3	-*x*+1/2, -*y*+3/2, -*z*+1/2
	-	-37.7	-26.8	-35.5	135.4	35.4	-*x* +1/2, *y*, -z+1
	-	-18.0	-3.3	-16.9	13.6	-24.6	-*x*+1/2, -*y*+1/2, -*z*+1/2
	-	-3.9	-0.6	-8.3	3.1	-9.6	-*x*, -*y*, -*z*+1
	-	2.9	-2.3	-20.3	12.0	-7.7	*x*, *y*+1, *z* / *x*, *y*-1, *z*
	-	-6.0	-7.2	-13.0	19.0	-7.2	*x*-1/2, -*y*, *z* / *x*+1/2, -*y*, *z*
Phase-I at ambient pressure – This work	#1	-76.3	-25.0	-15.2	60.8	-55.7	-*x*+1, -*y*+2, -*z*+1
	#2	-36.7	-12.7	-16.3	32.6	-33.0	*x*-1/2, -*y*+1, *z* / *x*+1/2, -*y*+1, *z*
	#3	-17.3	-3.3	-17.2	14.2	-23.6	-*x*+1, -*y*+1, -*z*+1
	#4	-4.3	-0.6	-8.9	3.5	-10.3	-*x*+1/2, -*y*+1/2, -*z*+3/2
	#5	-3.6	-1.3	-11.7	6.7	-10.0	-*x*+1, *y*-1/2, -*z*+3/2 / -*x*+1, *y*-1/2, -*z*+3/2
	#6	3.3	-2.5	-19.9	11.9	-7.2	*x*, *y*+1, *z* / *x*, *y*-1, *z*
Phase-I at 0.3 GPa – This work	#1	-80.5	-27.7	-15.7	67.7	-56.3	-*x*+1, -*y*+2, -*z*+1
	#2	-40.5	-14.6	-17.5	39.1	-33.5	*x*-1/2, -*y*+1, *z* / *x*+1/2, -*y*+1, *z*
	#3	-19.3	-3.9	-18.6	18.0	-23.9	-*x*+1, -*y*+1, -*z*+1
	#4	-5.1	-0.9	-10.4	5.2	-11.1	-*x*+1/2, -*y*+1/2, -*z*+3/2
	#5	-4.7	-1.9	-13.8	9.8	-10.5	-*x*+1, *y*-1/2, -*z*+3/2 / -*x*+1, *y*-1/2, -*z*+3/2
	#6	1.9	-3.3	-22.7	17.2	-6.9	*x*, *y*+1, *z* / *x*, *y*-1, *z*
Phase-II at 0.2 GPa – This work	#7	-23.0	-7.0	-13.1	16.2	-26.9	*x*-1, *y*+1, *z* / *x*+1, *y*-1, *z*
	#8	-27.6	-10.8	-8.6	27.5	-19.5	-*x*+1, *y*+1/2, -*z*+1/2 / -*x*+1, *y*-1/2, -*z*+1/2
	#9	-5.5	-3.3	-17.6	10.2	-16.2	*x*, *y*+1, *z* / *x*, *y*-1, *z*
	#10	0.4	-4.0	-33.0	23.4	-13.2	*x*+1, *y*, *z* / *x*-1, *y*, *z*
	#11	-2.8	-1.2	-9.6	5.8	-7.7	*x*-1/2, *y*-1/2, *z*+1 / *x*+1/2, *y*-1/2, *z*+1
	#12	-0.8	-1.1	-7.9	4.8	-5.1	*x*+1/2, -*y*-3/2, -*z*+1 / *x*-1/2, -*y*-3/2, -*z*+1

Table 3. Total energy breakdown for the six most energetically significant interactions in SALMID01, salicylamide-I at ambient pressure and 0.3 GPa and salicylamide-II at 0.2 GPa. Energies are calculated using the PIXEL method and are given in $kJmol^{-1}$.

Non-covalent interactions are listed in Table 2. Also included are estimates of the energies of each intermolecular interaction as calculated by the PIXEL method.[35, 49, 50] A breakdown of each energy is available in Table 3. Note that

PIXEL treats interactions at a *molecular* and not at an atomic level, and one must beware of falling into the trap of attributing a particular contact energy to a single prominent interatomic interaction, such as a hydrogen bond. Each molecule forms one intramolecular H-bond from the hydroxyl group to the amidic oxygen (O2H7…O1) and two intermolecular H-bonds (N1H5…O1 and N1H6…O2) (Table 2). N1H5…O1 forms across an inversion centre to create a dimer with a ring motif, graph set descriptor $R^2_2(8)$[51] (Figure 1, Table 2). The two molecules involved in each dimer are almost coplanar with a distance between least squares planes of 0.13 Å. This is the strongest interaction in the structure; the N…O distance is 2.923(3) Å and according to the PIXEL calculations the total intermolecular interaction energy is -55.7 kJmol^{-1} (labeled interaction #1 in Table 2). N1H6…O2 (interaction #2 in Table 2) connects the dimers along the *a*-axis via glide symmetry; the N…O distance is 3.000(2) Å and the molecule-molecule energy is estimated to be -33.0 kJmol^{-1}.

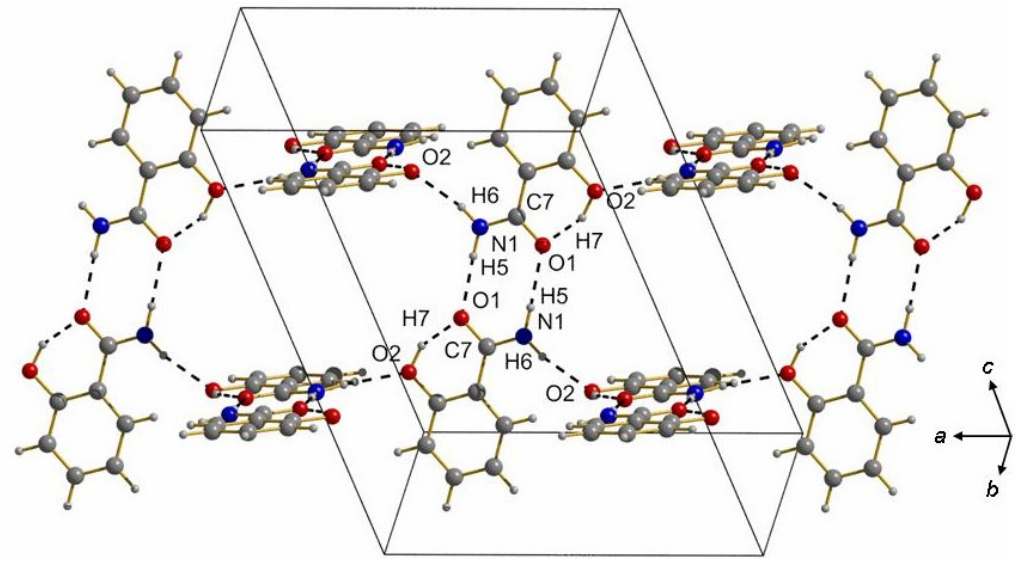

(a)

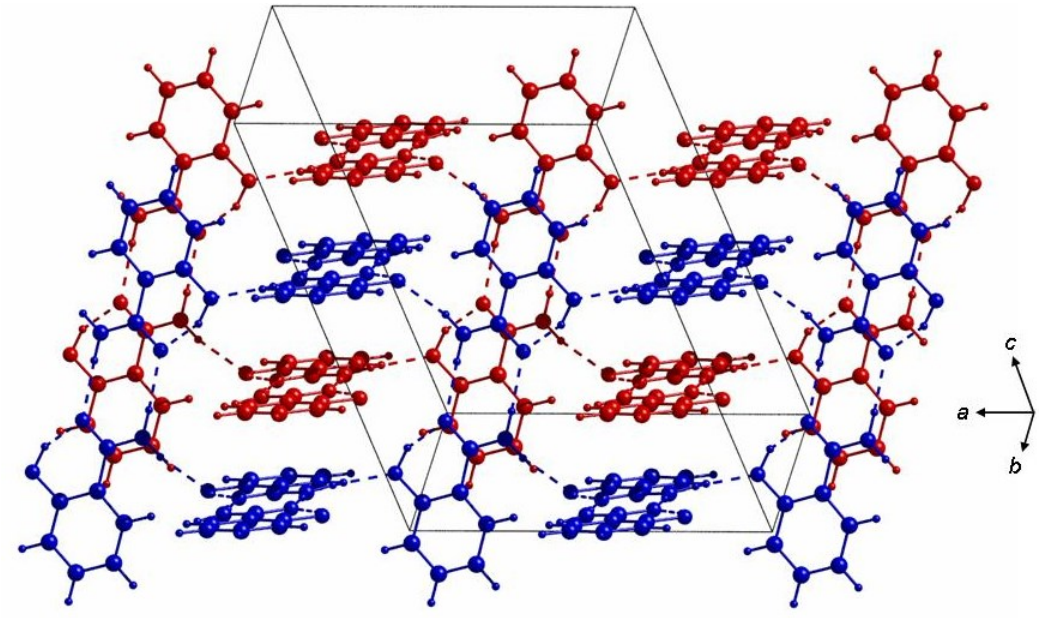

(b)

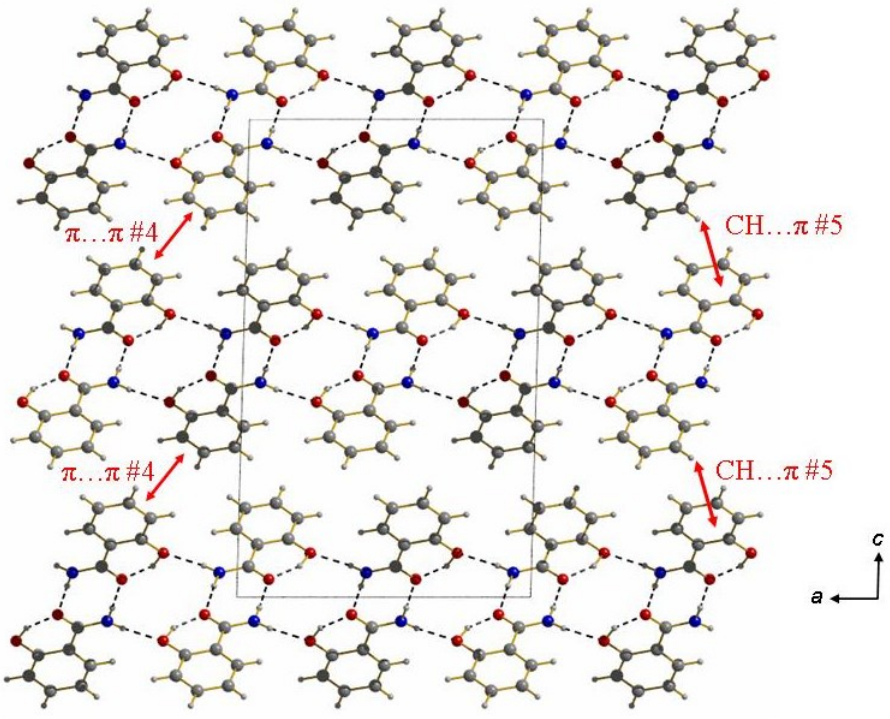

(c)

Figure 1. a) Hydrogen bonding in salicylamide-I creates an 'open' network of dimer interactions. b) Two networks combine via π…π stacking interactions to form slabs parallel to the *ab* plane. c) Slabs are connected to each other along the *c*-axis via π-interactions. Labels #4 and #5 refer to interactions studied using the PIXEL method (see Tables 2 and 3). The view of the π…π stacking is somewhat compromised by the perspective: the stacking distance is 2.68 Å with a large off-set of 5.09 Å at ambient pressure.

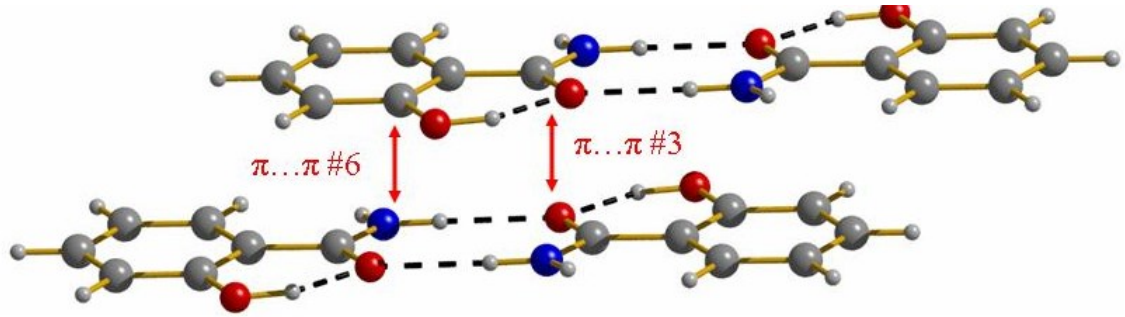

Figure 2. The π...π stacking interactions between the $R_2^2(8)$ dimers formed within the slabs in salicylamide-I. Labels #3 and #6 refer to the interactions studied using the PIXEL method (Tables 2 and 3).

The hydrogen bonding creates a rather 'open' network (Figure 1a) and efficient packing is achieved by the interweaving of two networks (coloured red and blue in Figure 1b). The networks interact by the two stacking interactions labelled #3 and #6 in Table 2 and illustrated in Figure 2. Interaction #3 is relatively strong for a stacking

interaction (-23.6 kJmol^{-1}), a feature which can be traced to large the electrostatic component (an energy breakdown is given in Table 3). Hirshfeld shape-index[2] plots[37] (Figure 3) indicate that the interaction occurs between highly polar amide groups at points *a* and *b* in Figure 3a, placing NH_2 groups directly on top of C=O groups. The electrostatic complementarity of these regions is very clear when the Hirshfeld surface is colour-coded according to the electrostatic potential (Figure 3b).[52]

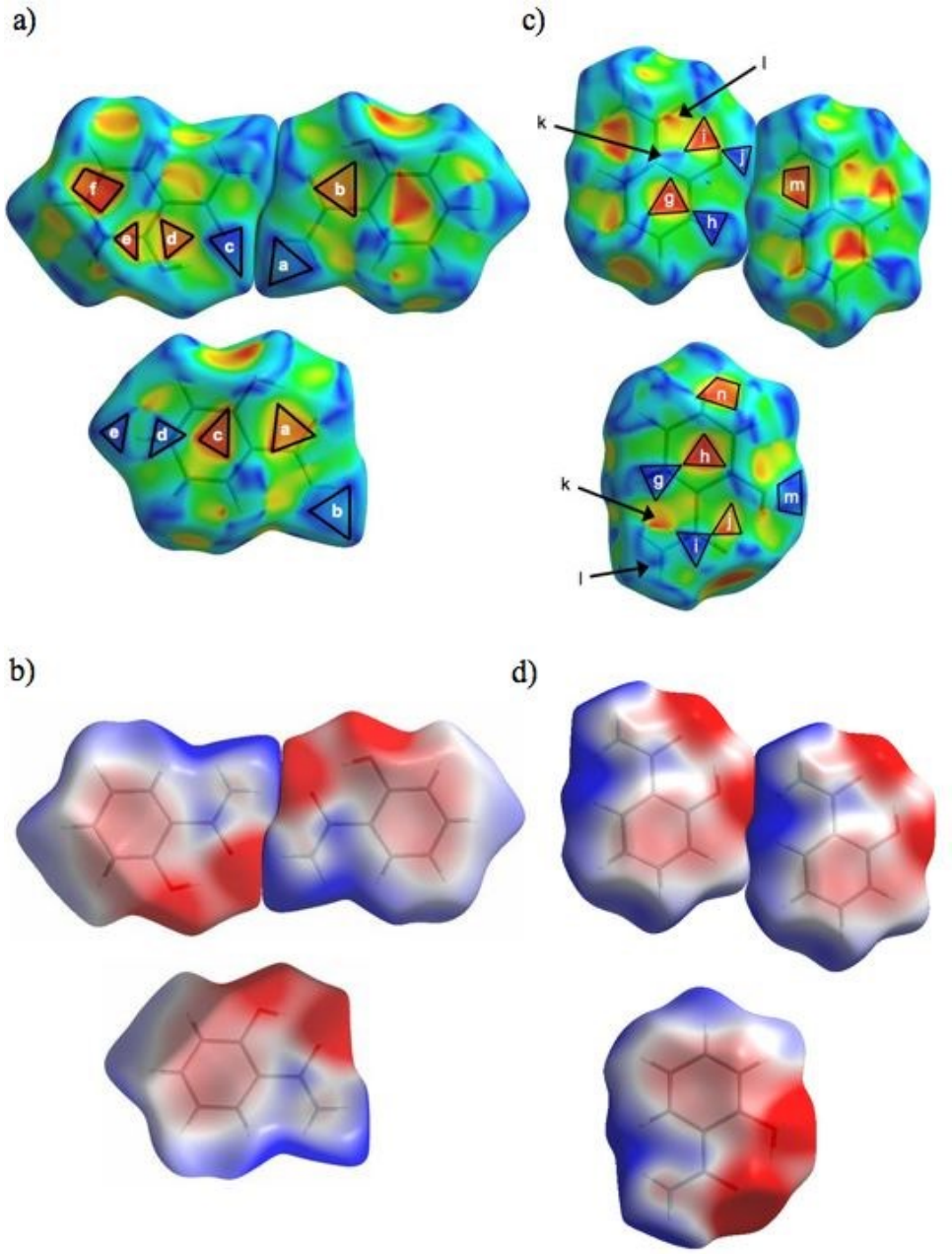

Figure 3. a) Shape index plots illustrating the contact points of interactions #3 and #6 in salicylamide-I. The same surfaces are shown in (b) with electrostatic potential mapped onto them in blue (+ve charge) and red (-ve charge). c) Shape index plots illustrating the contact points of interactions #9 and #10 in salicylamide-II, also with corresponding electrostatic potential plots in (d).

[2] Hirshfeld surfaces provide a useful way of looking at the packing environment in a crystal structure. The surface is created by applying the Hirshfeld stockholder partitioning method to divide the crystal into regions in which the electron density of the crystal is dominated by the electron density of a specific molecule. A number of useful properties can be mapped onto the surface including d_e (distances to nearest external atom) and d_i (distances to nearest internal atom) and the electrostatic potential. Patterns of π…π contacts can be illustrated by mapping the *shape index* onto the Hirshfeld surface; this is determined using the principal curvatures of the surface and shows concave regions as negative (red) and convex regions as positive (blue). Concave and convex regions in one surface fit into the convex and concave regions on a contacting surface.

Interaction #6 is a more typical stacking contact which is dominated by dispersion (Table 3). It is formed through points *c*, *d* and *e* on the Hirshfeld shape index surface (Figure3a). The contact is offset so that centre of the phenyl ring on one molecule is positioned over the carboxyl group on the other.

The pairs of H-bonded networks yield slabs, which are connected along the *c*-axis via off-set π…π and CH… π interactions (#4 and #5 in Figure 1c, respectively), which both have energies of *ca.* -10 kJmol^{-1} (Table 3). Dispersion is the largest component in the energy breakdown for both interactions. The CH…π contact in interaction #5 is labelled *f* in the Hirshfeld shape index plot of Figure 3a.

Compression of salicylamide-I to 5.1 GPa

Increasing hydrostatic pressure on salicylamide-I produces an anisotropic response in the unit cell parameters (Figure 4a). The greatest reduction occurs in the length of the *c*-axis (the slab-stacking axis) which decreases by 14.5% from ambient conditions to 5.1 GPa, whilst the *a*- and *b*-axes reduce by 4.7% and 4.1% respectively.

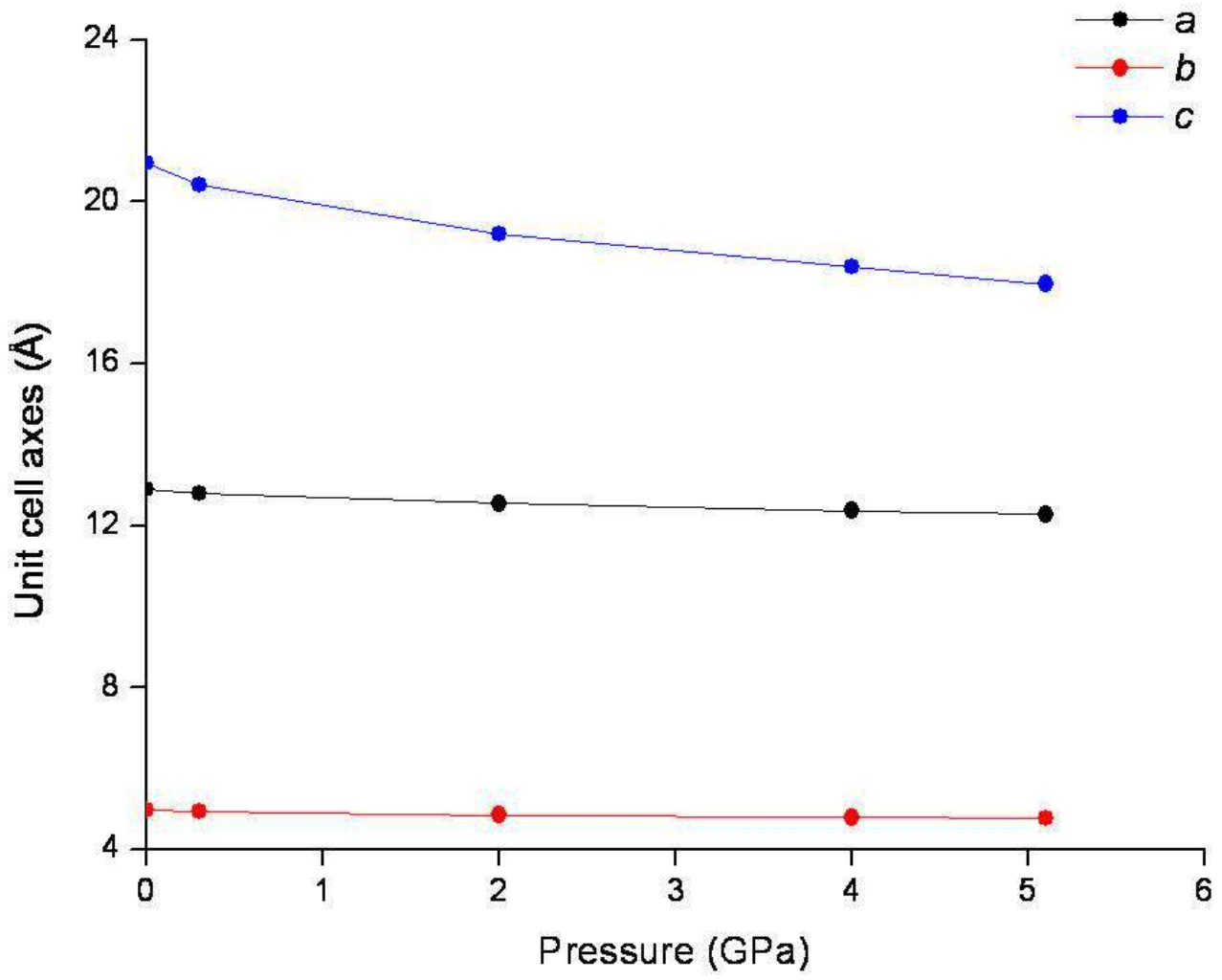

(a)

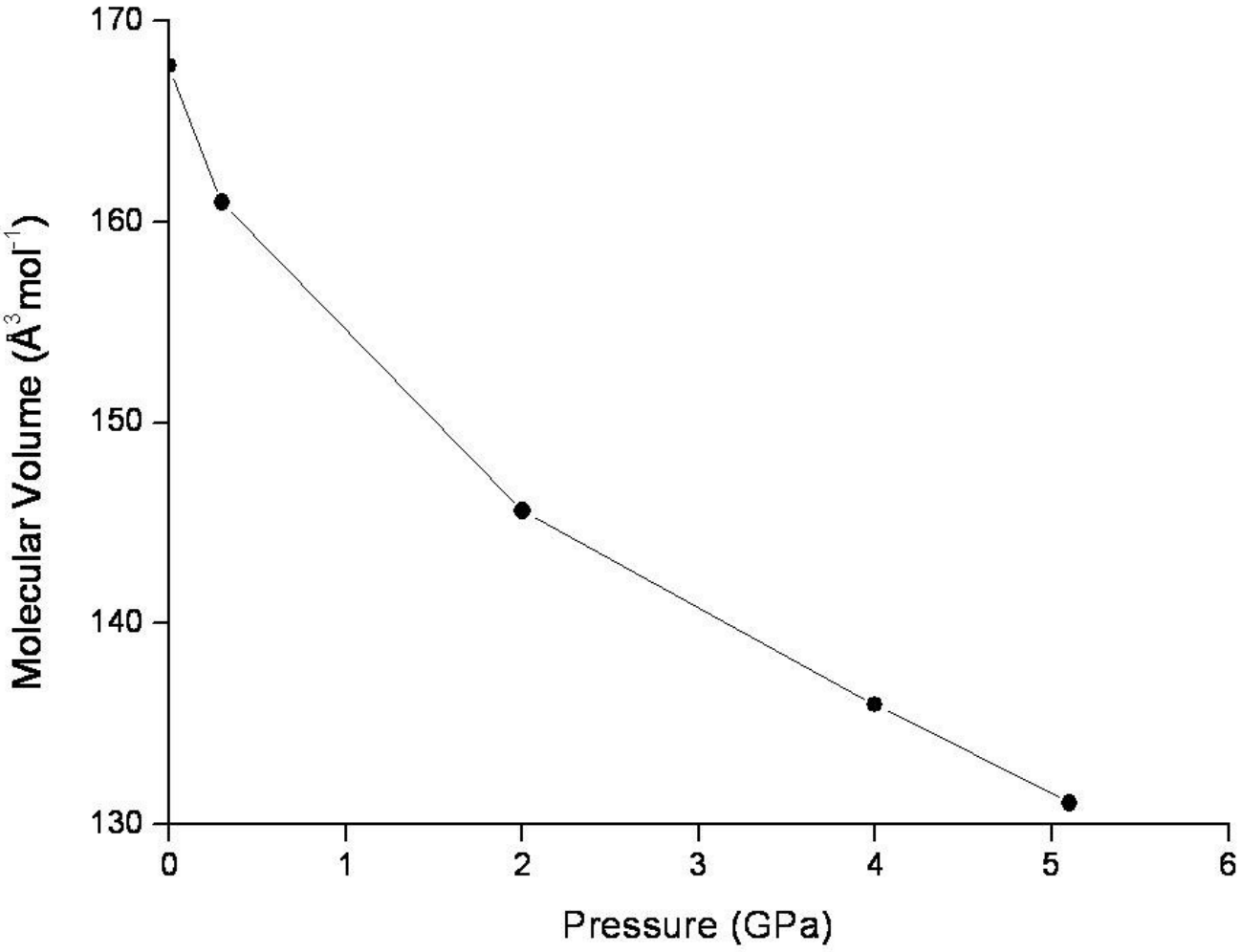

(b)

Figure 4. Variation of a) the unit cell parameters and b) the molecular volume of salicylamide-I as a function of pressure.

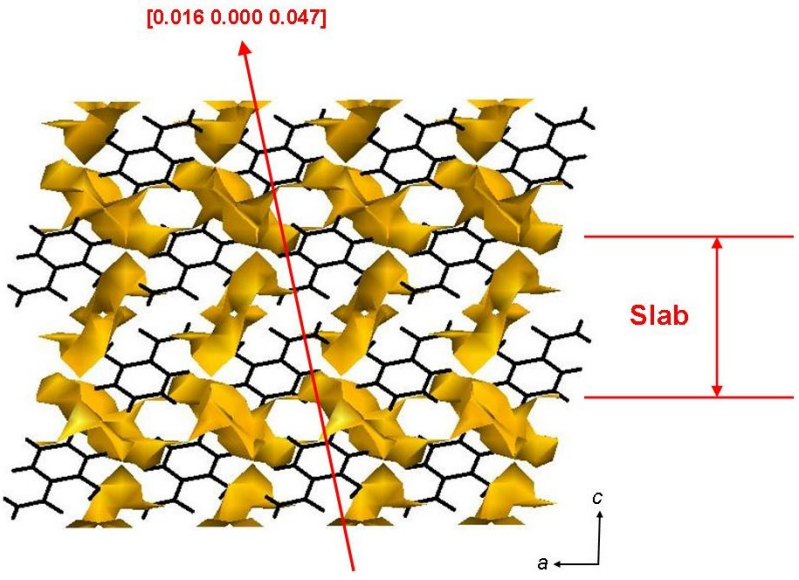

(a)

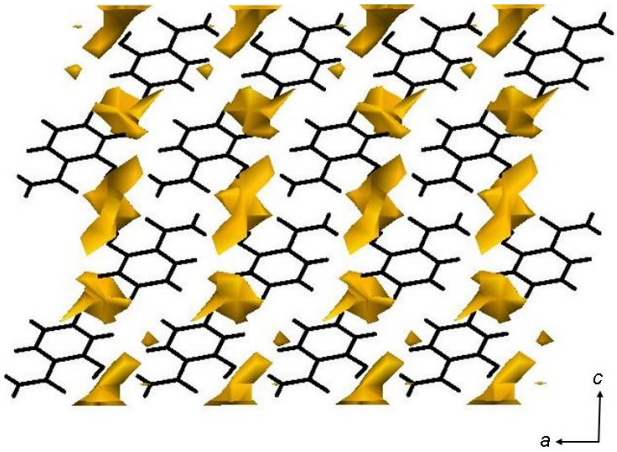

(b)

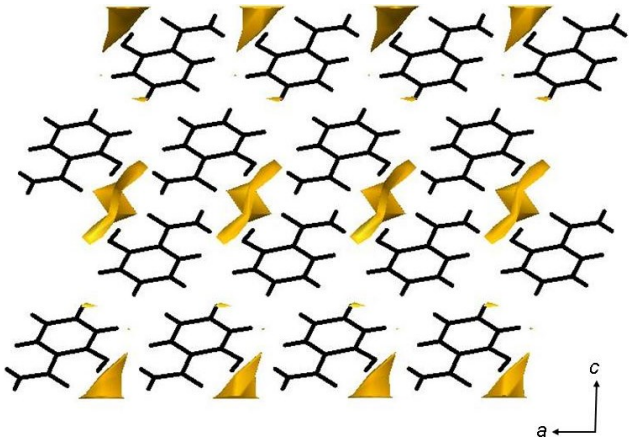

(c)

Figure 5. Void diagrams[40] of salicylamide-I at a) ambient conditions, b) 2.0 GPa and c) 5.1 GPa. Salicylamide molecules are coloured black. The vector which represents the direction of greatest compression is shown as a red arrow in a).

The direction of greatest linear strain lies along the direct space unit vector [0.016 0.000 0.047], which corresponds to the closing up of large voids in the structure which occur in and between the slabs of salicylamide dimers (Figure 5). As pressure is applied, the voids between the slabs close up more quickly than those within them and at 5.1 GPa the inter-slab voids have almost disappeared (Figure 5a-c). One eigenvector of the strain tensor must correspond to the *b*-axis by symmetry, and this is the direction of least compression in the structure. A Quicktime movie showing the compression of salicylamide-I when viewed along the *b*-axis is included in the supplemental material (file movie_layers_viewed_along_b.mov), and they clearly show that the most prominent effect of pressure is to push the slabs closer together.

The effect of pressure on the molecular geometry is small: the largest change occurs for τ(C3-C2-C7-N1), which is 1.7(3)˚ at ambient conditions and -4.9(5)˚ at 5.1 GPa. The hydroxyl oxygen also moves out of the plane of the ring:

τ(O2-C1-C6-C5) is 179.8(2)˚ at ambient conditions and 176.7(3)˚ at 5.1 GPa. The combination of these two factors affects the intramolecular hydrogen bond O2H7…O1, which compresses by a little less than 2% as pressure is increased to 5.1 GPa (Table 2). The two intermolecular hydrogen bonds are not constrained by the rigidity of the molecule: N1H6…O2 and N1H5…O1 compress by 8.8% and 5.6% respectively as the molecules are forced closer together.

The π…π stacking interactions in salicylamide-I compress more than the hydrogen bonds (Table 2): inter-planar separations for interactions #3 and #6 both decrease by *ca.*15% up to 5.1 GPa. The offset distance for interaction #3 reduces from 6.551 Å at ambient conditions to 6.347 Å at 5.1 GPa, and for interaction #6, it increases from 3.655 Å to 3.811 Å as the $R^2_2(8)$ dimers slide relative to one another. The offset distance for π…π interaction #4 shortens by 14.6% upon compression to 5.1 GPa as the slabs of molecules are pushed closer together.

All of the interactions become weaker as pressure is increased, and the variation of their energy with centroid-centroid distance is given in Figure 6. The graph shows that interactions #4 and #5 are relatively unchanged upon compression despite the closing of large voids between slabs. The slopes for interactions #1, #2, #3 and #6 all become much steeper as pressure increases; indicating that they are all becoming weaker as they are driven into the repulsive region of the intermolecular potential. Interaction #6 becomes destabilising above a pressure of 2.0 GPa; the contact has become very short with an inter plane distance of 2.859 Å at 5.1 GPa (Table 2).

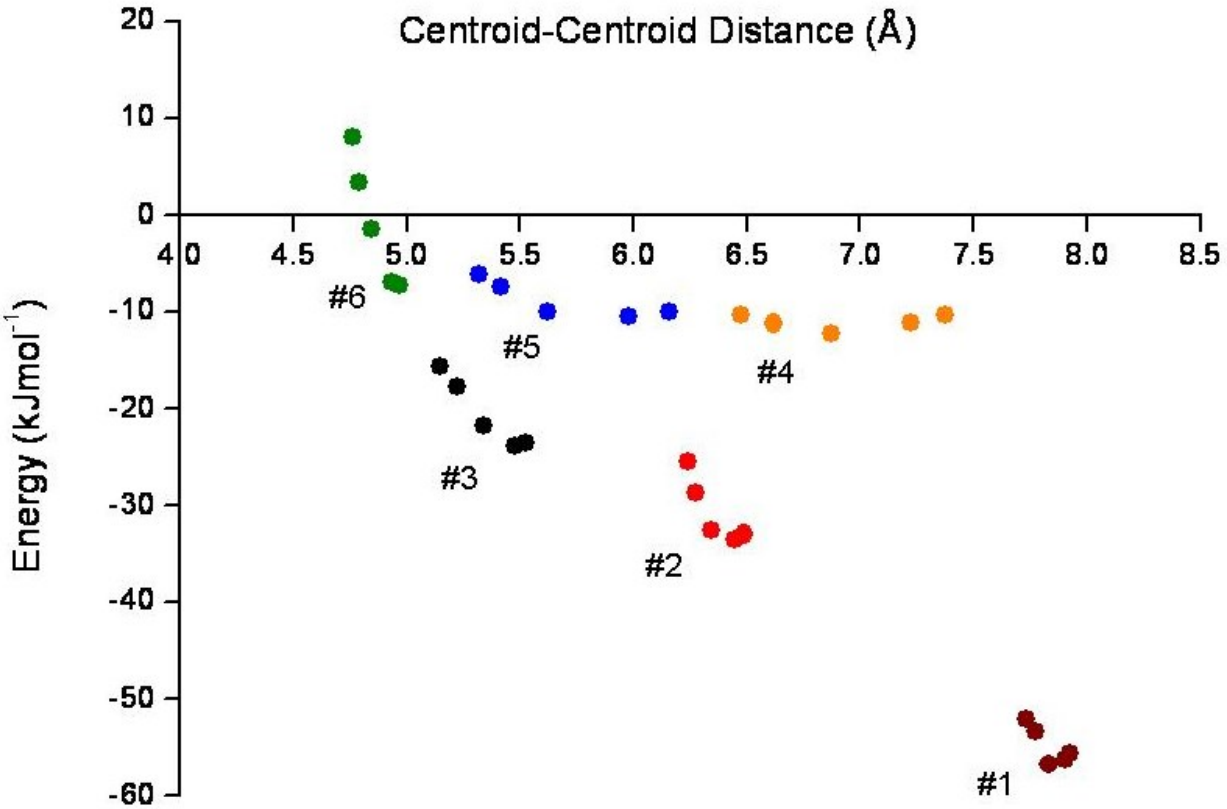

Figure 6. Graph of total interaction energy (in $kJmol^{-1}$) against the distance between the molecular centroids of the molecules involved in the interaction (in Å) in salicylamide-I. The numbers #1, #2 *etc.* refer to the contacts listed in Table 2.

In other systems,[10] energetic features like the ones described above have been observed prior to phase transitions; in addition beyond 5.1 GPa the diffraction profiles began to broaden significantly. Raman spectra were measured between ambient pressure and 5.8 GPa to determine whether a phase transition had occurred. Regrettably the results are somewhat ambiguous (Figure 7). Above 5.4 GPa a weak peak at 700 cm^{-1} increases in intensity and a weak shoulder develops at about 750 cm^{-1}. There is also a great reduction in peak intensity and sharpness between 5.0 GPa to 5.4 GPa. Such effects have been taken as indicative of phase transformations in other systems.[53, 54] By-and-large however, the spectra shown in blue and green towards the top of Figure 7 just look like broader, weaker versions of the spectra below. On balance we believe the broadening observed in the diffraction profiles is probably owed to build-up of strain in the crystal rather than a phase transition. Similar effects were seen in γ-glycine in the lead-up to a transition to the ε-phase.[12]

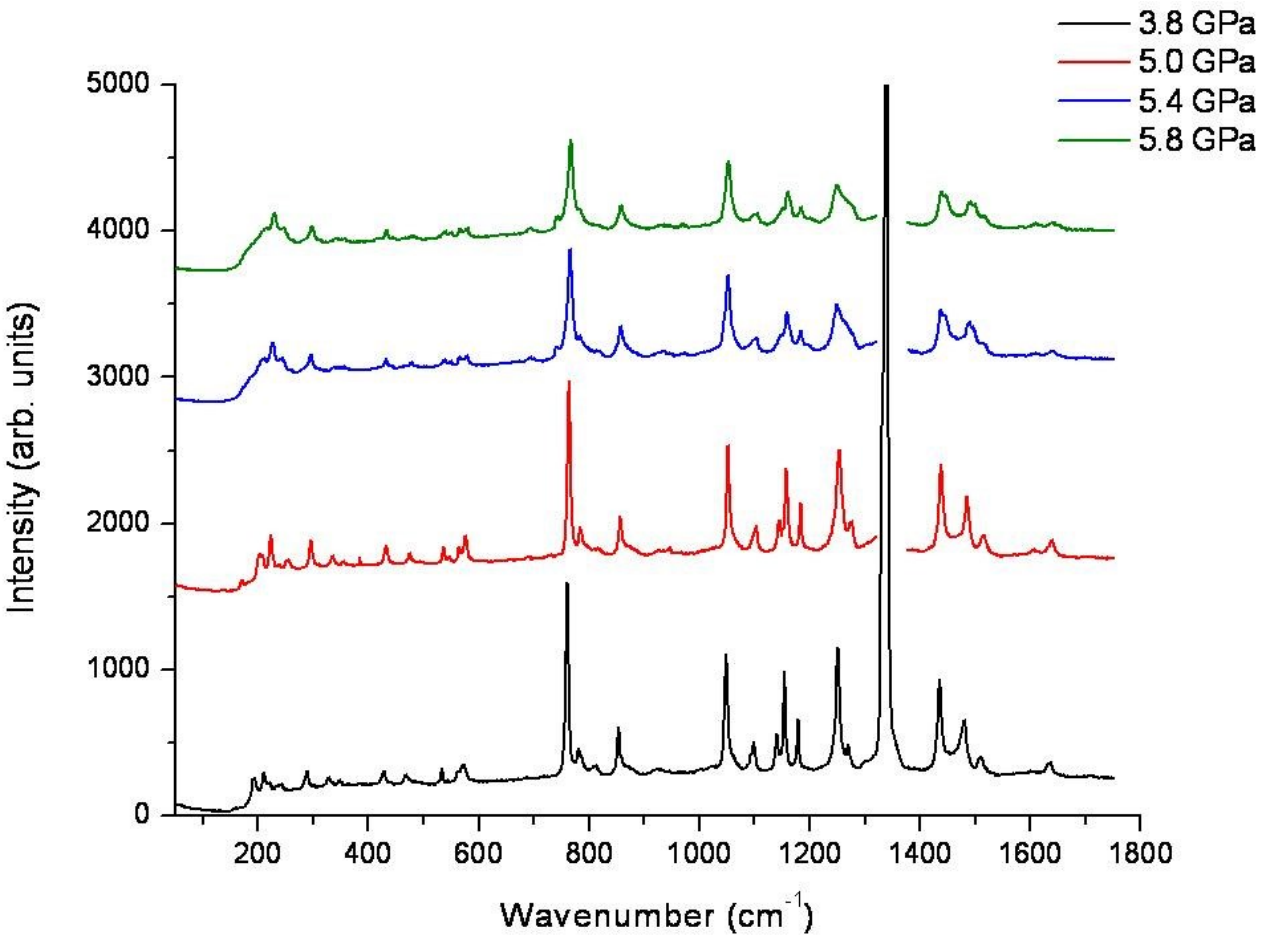

Figure 7. Raman spectra of compressed forms of salicylamide-I either side of 5.1 GPa. The intense peak at *ca.*1300 cm^{-1} is the diamond C-C stretch and is omitted from the red, blue and green spectra for clarity.

Salicylamide-II at 0.2 GPa

Pressure-induced recrystallisation of salicylamide at 0.2 GPa resulted in a new polymorph, hereafter designated salicylamide-II. The molecular conformation of salicylamide in phase-II is similar to that in phase-I at ambient

conditions: the largest difference in non-hydrogen-atom torsion angle is 4.1(6)˚, and arises from a twist in the amide group about the C2-C7 bond. This accords with *ab initio* calculations (GAUSSIAN03),[33] which show that the lowest frequency internal vibration in salicylamide is a twisting motion about the C2-C7 bond (75 cm^{-1}). The energy difference between the two conformations is thus very small (0.2 $kJmol^{-1}$).

PIXEL Interaction number	Interaction type	0.2 GPa
Intramolecular interactions		
-	**O2H7..O1[i]** H7…O1 O2…O1 <O2H7O1	 1.74(3) 2.530(5) 153(3)
Network-building interactions		
#7	**N1H6..O2[ii]** H6…O2 N1…O2 <N1H6O2 Energy	 2.26 3.027(4) 146 -26.9
#8	**N1H5..O1[iii]** H5…O1 N1…O1 <N1H5O1 Energy	 2.06 2.893(5) 157 -19.5
#9	**π...πi[iv]** Plane-plane Offset Energy	 2.633 4.898 -16.2
#10	**π...π[v]** Plane-plane Offset Energy	 3.375 1.942 -13.2
Slab-slab interactions		
#11	**C5H3...π** H3...π C5...π <C5H3π Energy	 3.80 4.682 157 -7.7
#12	**C4H2...π** H2...π C4...π <C4H2π Energy	 4.15 5.056 161 -5.1

Symmetry Operators:

i	*x,y,z*	v	1+*x, y, z*
ii	1+*x,* -1+*y,z*	vi	1/2+*x,* 3/2+*y,* 1-*z*
iii	1-*x,*1/2+*y,*1/2-*z*	vii	1/2+*x,* 1/2-*y,* 1-*z*
iv	*x,* 1+*y, z*		

Table 4. Geometry of intermolecular interactions in salicylamide-II. Distances are in Å, and angles in °. S.u's were calculated in PLATON. Total interaction energies are also included from PIXEL calculations and are given in $kJmol^{-1}$. For CH…π interactions, distances and angles are measured with respect to the centroid of the rings.

Structure Pressure	Coulombic	Polarisation	Dispersion	Repulsion	U	U_{adj}	H
SALMID01	-73.6	-37.3	-88.7	157.1	-42.5	-42.5	-42.5
Phase-I 0 GPa	-81.3	-29.0	-80.1	91.5	-98.9	-98.9	-98.9
Phase-I 0.3 GPa	-91.1	-34.0	-89.6	113.1	-101.6	-101.1	-67.9
Phase-II 0.2 GPa	-63.8	-24.6	-99.0	88.5	-98.9	-98.7	-76.1

Table 5. Components of the lattice energy and enthalpy for SALMID01, salicylamide-I and salicylamide-II. All energies are given in kJmol^{-1}. U_{adj} includes a correction for the small internal energy difference due to conformation change relative to ambient pressure structure. This was calculated in GAUSSIAN at the MP2/6-31G** level. Enthalpy values are calculated as $H = U + PV$, where P = pressure (in Pa) and V = molar volume (in m^{3}mol^{-1}).

Intermolecular interactions distances and angles along with PIXEL energy estimates are listed in Table 4; an energy breakdown is given in Table 3, while a summary of the total lattice energies in phases I and II is given in Table 5. Salicylamide-II features the same intramolecular hydrogen bond O2H7…O1 that is observed in phase-I, but because of the small conformational change, O…O distance is slightly longer [2.530(5) Å *vs.* 2.514(2) Å] (*cf* Tables 2 and 4). As in phase-I there are two intermolecular H-bonds; the identity of donor and acceptor atoms remains the same in both phases, but the symmetry relationships are different. An overlay of the H-bonding environment of the two phases is given in Figure 8. The molecules of salicylamide no longer form dimers: N1H5…O1 (interaction #8 in Table 4, -19.5 kJmol^{-1}) now links the molecules into a ribbon motif which runs parallel to the *b*-axis via a 2_1 screw axis (Figure 9a). N1H6…O2 (#7, -26.9 kJmol^{-1}) connects the ribbons into slabs via lattice translations along *a* (Figure 9b). In contrast to phase-I, the slabs in phase-II are formed by one H-bonded network only.

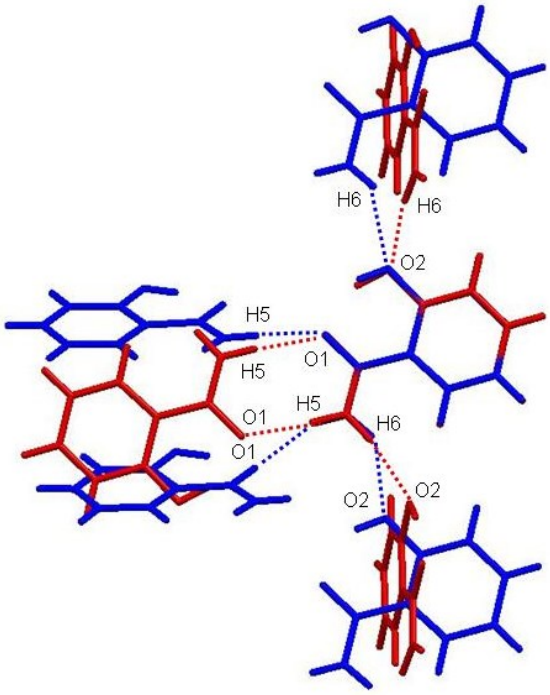

← ***Figure 8.*** Overlay of the H-bonding environments in salicylamide-I (red) and salicylamide-II (blue). Intramolecular O2H7…O1 H-bonds are omitted for clarity.

Intermolecular bonding within the slabs is re-enforced by π…π stacking interactions created by lattice repeats along the *b*- and *a*-axes; interactions are labelled as #9 and #10 in Figures 9a and b respectively. They have energies of -16.2 kJmol^{-1} and -13.2 kJmol^{-1}, respectively (Table 4), and these should be compared with -23.9 and -6.9 kJmol^{-1} in phase-I (at 0.3 GPa). Interaction #10, which, due to a small offset between the phenyl rings (1.944 Å), has a relatively large number of contact points on its shape index surface (labelled *g*-*l* in Figure 3c), whilst interaction #9 arises almost entirely from the point labelled *m*, which lacks the triangular shape typically observed for π…π stacking interactions. These contacts are all dominated by their dispersion terms (Table 3); the electrostatic components are weak, a feature which can be understood by considering the electrostatic potential surfaces shown in Figure 3d.

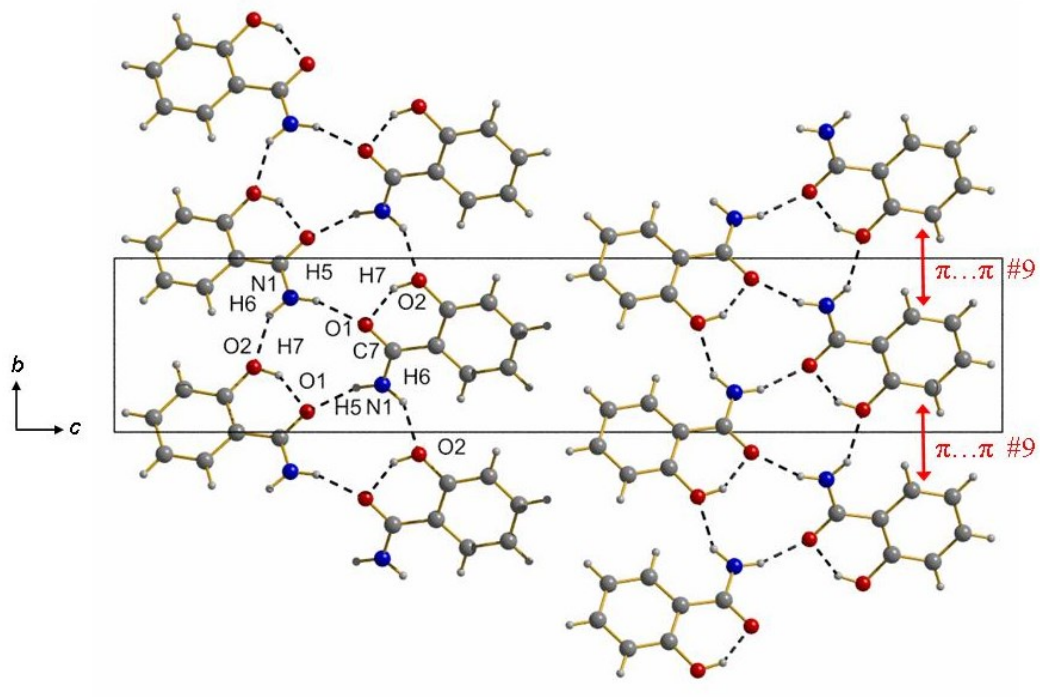

(a)

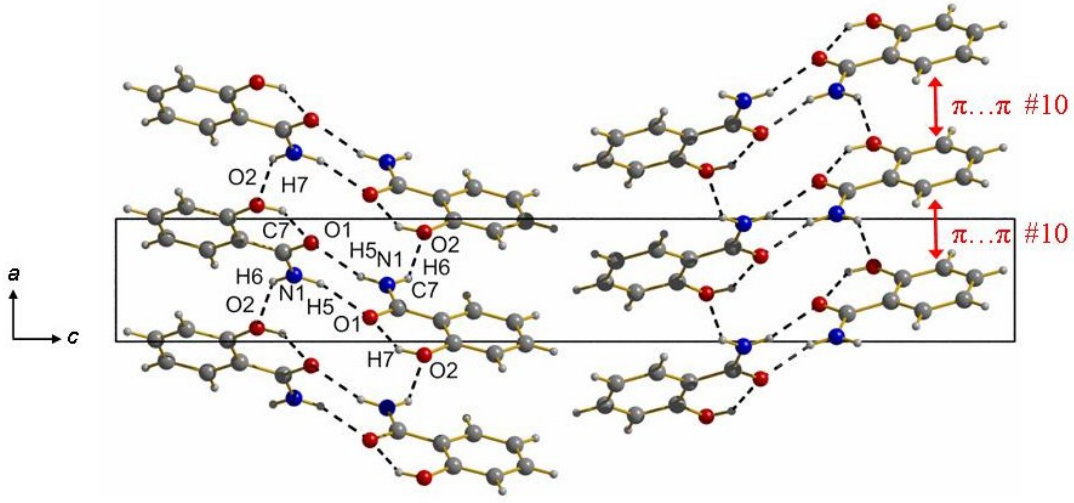

(b)

Figure 9. Salicylamide-II at 0.2 GPa, a) viewed along the *a*-axis and b) viewed along the *b*-axis. Labels 9 and 10 refer to the specific interactions studied in using the PIXEL method (Tables 3 and 4).

The slabs stack parallel to the (001) plane and each interacts with another along the *c*-axis through CH…π contacts (#11 and #12 in Table 4, the first of these is labelled *n* in Figure 3c). There are now no significant slab-slab π…π stacking interactions. PIXEL calculations show that the combined slab-slab interactions in Tables 2 and 4, are weaker in phase-II than phase-I at 0.3 GPa by 8.8 $kJmol^{-1}$.

Vibrational Contributions to the Thermodynamic Functions of Salicylamide-I and II

Periodic DFT calculations were carried-out on the structures of salicylamide-I and II obtained at 0.3 and 0.2 GPa, respectively, with the aim of obtaining zero point energies and the vibrational contributions to the enthalpy and entropy in the two phases at room temperature.

Inelastic neutron scattering data were collected on salicylamide-I at ambient pressure with the aim of validating the periodic DFT calculations. The positions of bands in an INS spectrum correspond to vibrational frequencies, as is also the case for IR and Raman spectroscopy. While intensities of IR and Raman bands are still rather difficult to calculate, in INS intensities depend only on the motions of the atoms. This means that both positions and intensities can be quite reliably calculated from a theoretical frequency calculation, making INS amongst the best techniques available for assessing the accuracy of periodic quantum mechanical calculations. A comparison of the observed and calculated INS spectra for salicylamide-I (calculated with the cell dimensions fixed to measured ambient pressure values) is shown in Figure 10. The agreement between observed and calculated frequencies is excellent, suggesting that the level of theory used here for determination of the thermodynamic properties of different phases of salicylamide is appropriate. By and large the intensities of the bands are also reproduced reasonably well; such disagreements as there are may be the result of over-estimation of factor group splitting.

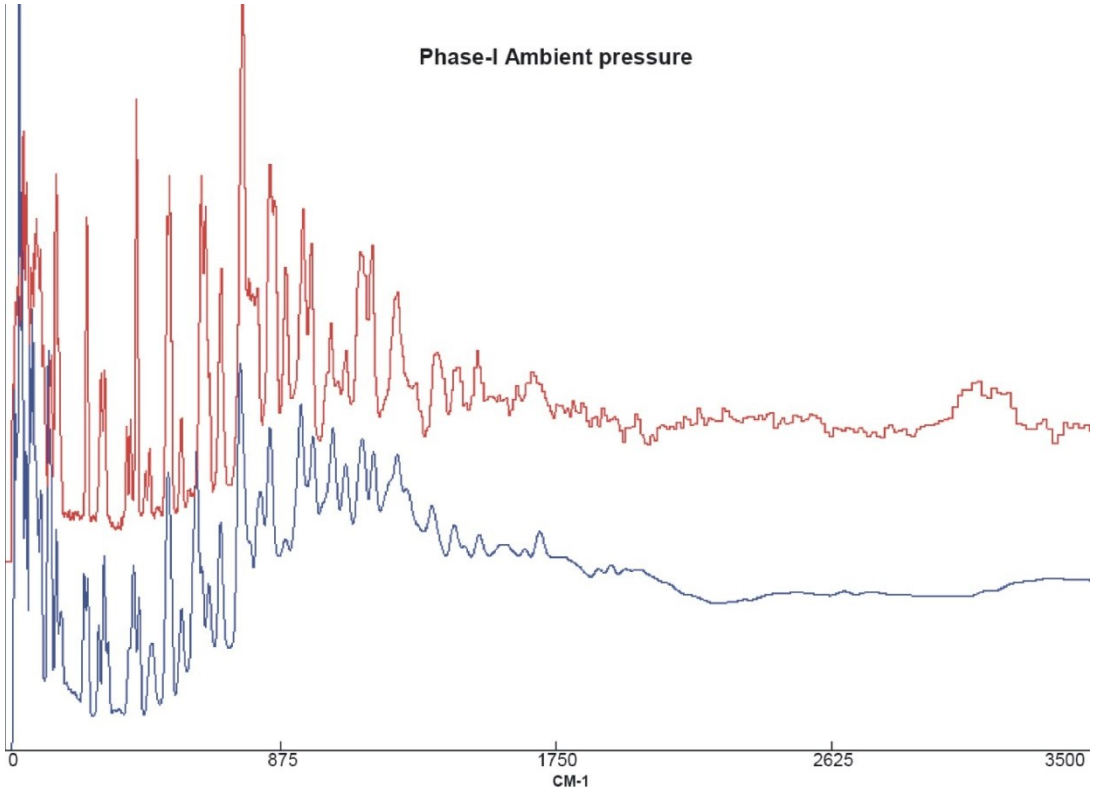

Figure 10. Observed (red) and calculated (blue) INS spectra for salicylamide-I at ambient pressure.

The largest deviation between the optimised and experimental non-H atomic positions in the crystal structures of salicylamide-I at ambient pressure and 0.3 GPa, and in salicylamide-II at 0.2 GPa, were 0.049, 0.047 and 0.063 Å, respectively. This excellent level of agreement also validates the theoretical approach used.

The values of the zero-point energy and the vibrational contributions to enthalpy, entropy and the free energy were calculated from the vibrational frequencies using standard formulae of statistical thermodynamics (see, for example, Equ 12.2, 12.9 and 12.16 in ref [55]), and these quantities are listed in Table 6.

Phase	ZPE/kJ mol^{-1}	*H*/kJ mol^{-1}	*S*/J mol^{-1} K^{-1}	*G*/kJ mol^{-1}
I at 0.3 GPa	343.58	22.99	152.35	321.14
II at 0.2 GPa	342.52	23.82	163.64	317.55
II - I	-1.06	0.83	11.292	-3.59

Table 6. Vibrational contributions to the thermodynamic functions at 298.15 K for salicylamide phases I and II calculated using harmonic frequencies obtained from periodic DFT calculations. ZPE = zero point energy.

Discussion

The Crystal Structure of Salicylamide at Ambient Pressure

Interactions 1-6 in phase-I (Table 2) can be categorised as (*i*) intra-network (hydrogen bonding within networks; contacts #1 and #2), (*ii*) network-network (interactions which occur within slabs, between different networks; contacts #3 and #6), and (*iii*) slab-slab (interactions occurring between slabs; contacts #4 and #5). On average, the interactions which form the networks are stronger (Table 3) than the slab-building interactions which form between the networks, and these, in turn, are stronger than the interactions between the slabs.

The lattice energy calculated for the CSD entry SALMID01 is -42.5 kJmol^{-1} (Table 5), and is much less stable than the structure of salicylamide-I reported here (-98.9 kJmol^{-1}). The latter is in very good agreement with the literature sublimation enthalpy values of 101.9(4) kJmol^{-1},[56] and 99.3(23) kJmol^{-1}.[57] The difference between the two models lies in the location of the origin on either one of the two crystallographically distinct inversion centres in space group *I*2/*a*. We assume that a non-standard setting must have been used for the refinements quoted in references [17] and [18], though no mention of this is made in either publication.[3] The structures of both proposed models consist of slabs of molecules connected by π-interactions. However, the instability of SALMID01 results from the large repulsive component (Table 5), which arises because of a number of short H…H contacts at *ca*.1.96 Å (X-H distances normalised to standard neutron values) which occur between slabs. Though not unprecedented, these distances are very short by comparison of other H…H distances in the Cambridge Database (see Figure 6 in ref. [58]), and there is a large repulsive contribution of 135.4 kJmol^{-1} to this contact which is destabilising with an overall energy of +35.4 kJmol^{-1} (Table 3, top section). Indeed, it was the existence of these short H…H interactions which first attracted our interest in the behaviour of salicylamide at high pressure!

[3] We have contacted Dr. Pertlik, the author of the second of these papers, but regrettably the original diffraction and refinement data have been lost.

The information that is contained in a Hirshfeld surface analysis can be condensed into a 2D histogram of d_i (x-axis) against d_e (y-axis) known as a *fingerprint plot* which is useful for observing packing differences between structures.[37, 59] The fingerprint plot for SALMID01 is shown in Figure 11a. This plot looks quite bizarre by comparison with examples of other H-bonded solids quoted in reference [37]. For example the feature which is circled in red indicates the presence of numerous very short H…H contacts. The strangeness of the fingerprint plot supports our contention that the coordinates quoted in the two previously published crystal structures of salicylamide are incorrect (at least with respect to the usual setting of the space group).

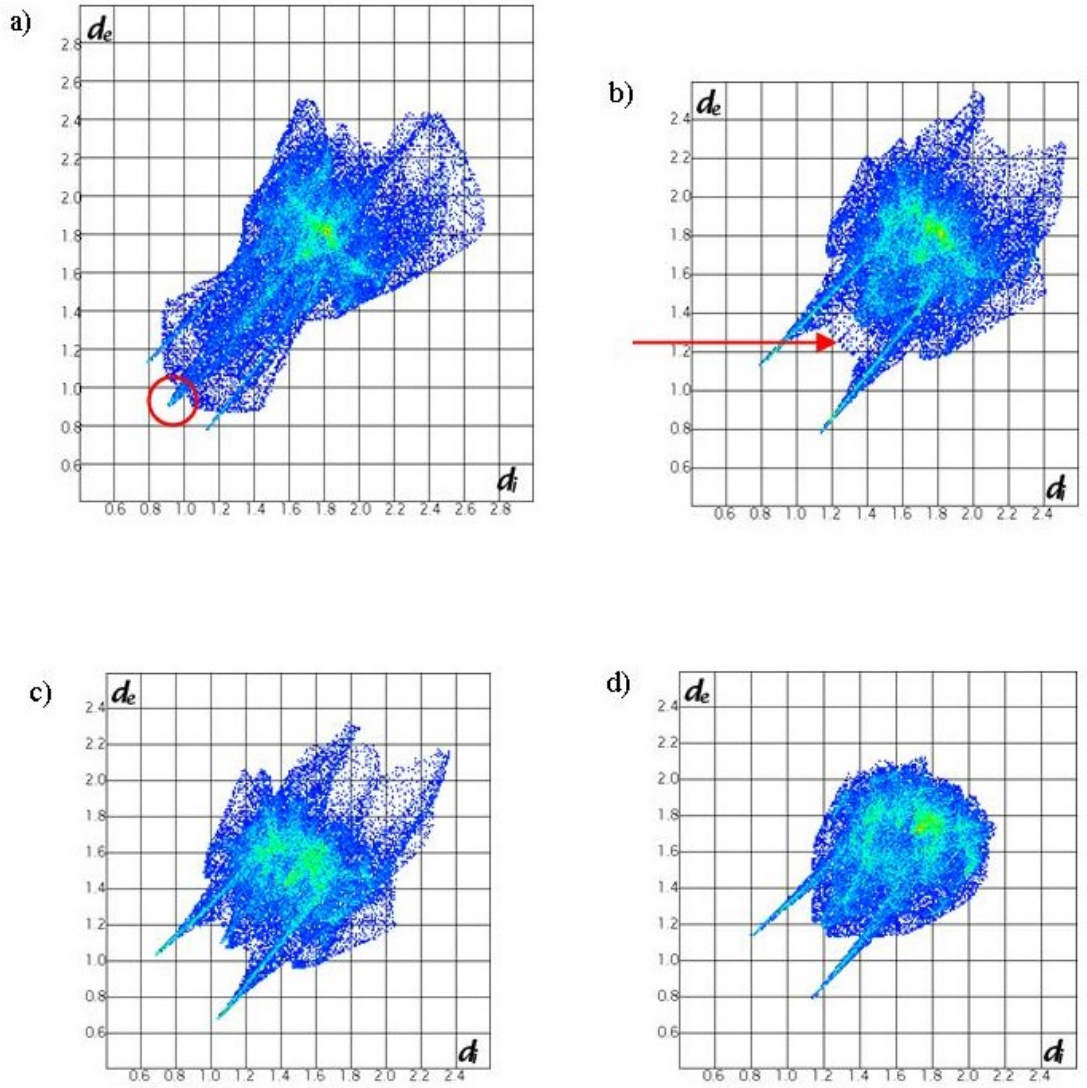

Figure 11. Fingerprint plots: a) SALMID01[18] (red circle indicates an elongated nose region due to short intermolecular H…H contacts), b) salicylamide-I at ambient conditions (the red arrow points towards a region corresponding to short H…H contacts across a dimer), c) salicylamide-I at 5.1 GPa, d) salicylamide-II at 0.2 GPa.

The fingerprint plot for our model of the crystal structure of salicylamide, which is shown in Figure 11b, is more normal for H-bonded materials.[37] Two prominent 'prongs' are characteristic of NH…O H-bond formation, while the 'skirt' of points (indicated with a red arrow) between the prongs derive from short H…H contacts formed across the

$R^2_2(8)$ dimers. The various π…π contacts are represented by the green area in the middle of Figure 11b. The compression of salicylamide-I results in the shortening of contacts, and Figure 11c shows that overall, the fingerprint plot moves towards the origin upon compression to 5.1 GPa. A feature develops in the skirt region as H…H contacts shorten. Development of short H…H contacts is characteristic of compressed organic crystal structures.[58]

Formation of Salicylamide-II at 0.2 GPa

Salicylamide-II was grown *in-situ* by recrystallisation of a saturated solution at pressure. Crystal growth resulted in three crystallites and reflections were harvested from all three crystallites. Refinement of the merged data resulted in a completeness of over 90% whereas integration of one domain alone gave a completeness of *ca*. 30%. This is a good example illustrating a situation where use of a multiple sample (or a twinned crystal) can be beneficial: high-pressure datasets often suffer from low completeness because of shading from the steel pressure cell body, and inclusion of multiple crystals in different orientations within the gasket hole can improve this.

Whereas phase-I crystallises in the centrosymmetric space group *I*2/*a*, phase-II forms in the Sohncke group $P2_12_12_1$, which is relatively unusual for achiral molecules.[60] Inversion centres are very common features in crystal structures of achiral compounds, but if a molecule has approximate mirror or inversion symmetry an inversion relationship can be mimicked by a rotational operator. The appearance of a polymorph in $P2_12_12_1$ may be ascribable to approximate mirror symmetry of the planar and rigid salicylamide molecule,[60] which means that when nucleating the $P2_12_12_1$ structure does not have the problem of "rejecting" the wrong hand of molecule for the growing crystallite.

There is no evidence that phase-II is formed on compression of phase-I, and the only route by which we have observed it is via direct recrystallisation from solution at high pressure. It is important to recognise that transformations between very different crystal structures involving substantial reorganisation of the crystal packing are likely to be subject to a large activation barrier, and are kinetically hindered. The results on salicylamide imply that there is no energetically favourable route for transformation of phase-I directly into phase-II. Related features were observed in a study of the effect of pressure on different polymorphs of glycine.[12] α-Glycine remains in the same phase up to at least 6 GPa, and Raman data suggest that it is stable to over 20 GPa.[61] By contrast β-glycine transforms to δ-glycine at 0.8 GPa, and γ-glycine transforms to ε-glycine at 2 GPa. Thus the polymorph formed depends on the identity of the starting phase, and there is a close topological relationship between the β and δ forms and between the γ and ε-forms.[12]

The molecular structures in phases I and II are essentially the same. Both phases comprise slabs of hydrogen-bonded molecules which stack parallel to the (001) plane. The identity of the donor and acceptor atoms for the hydrogen bonds is the same in both cases, but the symmetry operations are different. This means that in phase-II the slabs are made up of a single hydrogen-bonded network, whereas in phase-I it was an inter-weaving of two networks. The density of phase-II is greater than phase-I at 0.3 GPa by 0.058 Mg m^{-3} (Table 1), which is nicely illustrated with the fingerprint plot in Figure 11d with the disappearance of the diffuse blue regions which represent long-range contacts across voids. The disappearance of the skirt region in Figure 11d represents the loss of the $R^2_2(8)$ dimers in phase-II.

Table 5 shows the intermolecular lattice energy values for both phases and a breakdown of energy terms: at 0.3 GPa, the overall cohesive energy of phase-I (-101.6 $kJmol^{-1}$) is slightly more negative than phase-II (-98.9 $kJmol^{-1}$).

Interpolation of the total intermolecular interaction energy for phase-I to 0.2 GPa (-100.7 kJmol^{-1}) suggests that the difference in cohesive energies is less at 0.2 GPa, *ca* 2 kJmol^{-1} in favour of phase-I. Comparison of the rows in Table 5 for phase-I at 0.3 GPa and phase-II at 0.2 GPa shows that phase-I is favoured by the Coulombic and polarisation terms, while phase-II is favoured by the dispersion and lower repulsion terms. This picture is unchanged if the phase-I energies are interpolated to 0.2 GPa (E_{Coul} = -87.4, E_{Pol} = -32.1, E_{Disp} = -87.0 and E_{Rep} = +104.8 kJmol^{-1}). It is interesting that even though phase-II is denser, its repulsion term is lower.

The differences in the Coulombic energies of phases I and II can be traced to differences in the most important Coulombic interactions, namely the H-bonds. The top interaction in phase-I is the dimer mediated by N1H5…O1 H-bonds. The electrostatic component of this bond is -80.5 kJmol^{-1}, but for the purposes of comparisons between different H-bonds this value should be halved (-40.3 kJmol^{-1}) as the interaction involves two H-bonds. In phase-II, the electrostatic component of the N1H5…O1 H-bonds is only -27.6 kJmol^{-1}. Though the N1H5…O1 H-bonds have similar N…O distances in phases I and II (Tables 2 and 4), that in phase-II is much less linear (157°) than in phase-I (176°). Moreover, N1-H5 vector is more closely aligned with the lone pair on O1 in phase-I than in phase-II. While the less ideal geometry of the H-bonding in phase-II likely contributes to the differences in the Coulombic energies, it is important to bear in mind that the figures quoted refer to whole molecule interactions, and not just the H-bonds, and it is not possible on the basis of the PIXEL results to ascribe the differences to changes in H-bond geometry alone.

The second strongest interaction in phase-I is N1H6…O2, which has a Coulombic component of -40.5 kJmol^{-1}, compared to -23.0 kJmol^{-1} for the related N1H6…O2 interactions in phase-II (Table 3). The N1…O2 distance is shorter, more linear and more optimally aligned with the O2 lone pair in phase-I.

The repulsion components of the H-bonds in phase-II are lower, but this is not enough to outweigh the differences in the Coulombic terms, and the H-bonds in phase-II are overall weaker than those in phase I by 15 kJmol^{-1}, and it would appear that the Coulombic advantage of phase-I can be traced to the more favourable H-bonding geometry in the structure. The data in Table 3 also show that, by contrast, the dispersion components of the various stacking and CH-π interactions in phase-II are both more numerous and more energetic than in phase-I. Broadly speaking, what is lost in H-bonding in phase-I is made up by improved dispersion interactions in phase-II.

The energy data in Table 3 and in the paragraphs above indicate that intermolecular interactions phases I and II are energetically competitive overall. In addition, the data in Table 1 show that phase-II is denser than phase-I, with a volume of 154.7 Å^3 per molecule at 0.2 GPa, compared to 161.0 Å^3 per molecule for phase-I at 0.3 GPa. Interpolation of the phase-I volume to 0.2 GPa gives a value of 163.3 Å^3 per molecule. This volume difference equates to a *PV* advantage of *ca* 1 kJmol^{-1} for phase-II at 0.2 GPa.

The *PV* term becomes a progressively more important contributor to free energy as *P* increases, and eventually it would be expected to outweigh the cohesive energy derived from efficient H-bonding. In the phase-I to II transitions in serine[62, 63] and serine hydrate[64] (both at 5 GPa), for example, the change in cohesive energy is actually positive, but this is out-weighed by the negative change in the *PV* term. In the transition from serine-II to III at 8 GPa H-bonds actually become longer, but there is an increase in H…H contacts pointing to enhanced dispersion terms. It is interesting to speculate that at very high pressures H-bonded polymorphs may become disfavoured relative to efficiently-packed structures dominated by dispersion.

Zero Point Energy and Vibrational Contributions to Free Energy

Hudson and co-workers have recently pointed-out that differences in zero point energy can be similar to, or even larger than, overall differences in polymorph energies.[65] It is therefore important to take zero point energies into account when discussing relative polymorph stabilities, particularly where H-bonding is involved as this has a strong effect on vibrational energies. In Hudson's study, it was shown that for glycine the dominant effect on ZPE differences between the α- and γ- polymorphs comes from the internal bending modes. These modes tend to deform H-bonds from linearity, and so they increase in frequency when H-bonding is strong and linear. Strong H-bonding can therefore act to destabilise a structure through this zero point energy contribution. On the face of it therefore, salicylamide-II, with its weaker H-bonding, should also be favoured over phase-I by a smaller zero point energy.

Vibrational frequencies of phases I and II were calculated using periodic DFT and used to estimate the vibrational contributions to the thermodynamic functions at 298.15 K. The results, which are listed in Table 6, show that indeed, the zero point energy of phase II of salicylamide is *ca*.1 kJmol^{-1} smaller than that of phase-I. Break-down of the contributions to the zero-point energy in the manner described by Hudson shows that the ZPE difference can be traced to lower vibrational frequencies of phase-II in the 0-400, 1000-1200, 1600-1800 and 2000-3000 cm^{-1} regions of the vibrational spectrum. The 0–400 cm^{-1} region consists mostly of whole molecule lattice vibrations, and it seems intuitively reasonable that these modes are lower in frequency in phase-II with its weaker H-bonding (see also below). The regions from 1000-1200 and 1600-1800 cm^{-1} contain rocking and bending modes centred on the NH_2 groups. As Hudson has observed in glycine, these modes are higher in frequency in phase-I because they lead to deformations of H-bonds which are more linear (and energetic) than in phase-II. The region between 2000 and 3000 cm^{-1} contains the stretching mode of the OH groups involved in internal OH…O H-bonding. This is higher in frequency in phase-I; the reason for this is not altogether obvious as the O…O distance is longer in phase-II, so that the OH stretch would be expected to be higher in phase-II.

Phase-II is also favoured by entropy, $T\Delta S$ is *ca* -3 kJmol^{-1} at 298.15 K. Entropic contributions drop-off quite rapidly with wavenumber, and the largest differences are seen in the lattice modes below about 200 cm^{-1}. As described above in the context of the ZPE, the lower frequencies in phase-II are consistent with a less rigid network of H-bonds.

The generally lower frequencies of phase-II mean that the vibrational enthalpy favours phase-I, but not enough to over-ride the contributions of the ZPE and entropy.

In summary, the formation of salicylamide-II at 0.2 GPa can be understood in terms of (a) the replacement of H-bonds by dispersion-dominated stacking and CH…π interactions; (b) its higher density and (c) its lower vibrational frequencies. The last of these occurs because of weaker H-bonding in phase-II which, paradoxically perhaps, gives this polymorph an advantage in both zero point energy and entropy.

Conclusions

We have shown that the published structures of salicylamide-I at ambient pressure, though not exactly wrong, appear to have been described with respect to a non-standard space group origin. The overall features of the published and revised structures are similar: the molecules are connected through H-bonding into layers, and these layers are then

stacked through π-π interactions. However, our structure does not contain the short H…H contacts which were a notable feature of the previously proposed structure. Packing energy calculations using the PIXEL method and Hirshfeld surface analysis were both very useful for verifying the structure of salicylamide-I presented here.

Application of pressure to salicylamide-I up to 5.1 GPa does not result in any phase transitions, though the interactions within the layers do enter a destabilising region of their potentials. Above 5 GPa the crystal appears to deteriorate. Although this behaviour is usually taken to imply that a transition has occurred, Raman spectra taken after the collapse are rather similar to those taken at lower pressures, and while we are not able to make a definitive comment on the phase of the collapsed material, we are not convinced by the suggestion that a phase transition has occurred. .

When a crystal of salicylamide is grown directly from solution at 0.2 GPa a new high-pressure phase, salicylamide-II, is formed. The structure was determined from data collected on a sample consisting of three crystallites, and the data set had an unusually high completeness for a high-pressure structure determination.

Our aim in this paper has been to establish what makes the new form energetically competitive with phase-I. PIXEL calculations show that although phase-II features similar NH…O_{phenol} and NH…O_{amide} interactions to those present in phase-I, these interactions are substantially weaker. This deficit in the cohesive energy is made-up by increases in the strengths of π-π and CH…π interactions in phase-II, and at 0.2 GPa the cohesive energies favour phase-I by *ca.* 2 $kJmol^{-1}$. However, phase-II is denser than phase-I, and the lower molecular volume gives phase II an advantage of 1 $kJmol^{-1}$ via the *PV* contribution to its free energy. Finally, DFT frequency calculations (validated by experimental inelastic neutron scattering data) show that the zero point energy of phase-I is *ca.* 1 $kJmol^{-1}$ higher than phase-II because in phase-I the frequencies of NH bending modes are increased by the need to deform strong, linear NH…O hydrogen bonds. The presumably more rigid H-bonding network of phase-I also means that its low frequency phonon modes are higher in energy than in phase-II, and this leads to an entropic advantage of some 3 $kJmol^{-1}$ for phase-II. Entropy is often neglected when comparing the thermodynamic stabilities of different polymorphs, but in the present study it is the largest of all terms considered.

Overall we estimate that at 0.2 GPa and room temperature the free energy of phase-II is lower than that of phase-I by about 3 $kJmol^{-1}$.

References

[1] D. R. Allan and S. J. Clark, *Physical Review B: Condensed Matter and Materials Physics*, 1999, **60**, 6328-6334.

[2] D. R. Allan and S. J. Clark, *Physical Review Letters*, 1999, **82**, 3464-3467.

[3] D. R. Allan, S. J. Clark, M. J. P. Brugmans, G. J. Ackland and W. L. Vos, *Physical Review B: Condensed Matter and Materials Physics*, 1998, **58**, R11809-R11812.

[4] I. D. H. Oswald, D. R. Allan, G. M. Day, W. D. S. Motherwell and S. Parsons, *Crystal Growth & Design*, 2005, **5**, 1055-1071.

[5] S. A. Moggach, S. Parsons and P. A. Wood, *Crystallography Reviews* 2008, **14**, 143-184.

[6] F. P. A. Fabbiani and C. R. Pulham, *Chemical Society Reviews*, 2006, **35**, 932-942.

[7] S. A. Moggach, T. D. Bennett and A. K. Cheetham, *Angew. Chem. Int. Ed.*, 2009, **48**, 7087-7089.

[8] D. R. Allan, A. J. Blake, D. Huang, T. J. Prior and M. Schroeder, *Chemical Communications*, 2006, 4081-4083.

[9] S. A. Moggach and S. Parsons, *Specialist Periodic Reports: Spectroscopic Properties of Inorganic and Organometallic Compounds*, 2009, **40**, 324-354.

[10] P. A. Wood, R. S. Forgan, D. Henderson, S. Parsons, E. Pidcock, P. A. Tasker and J. E. Warren, *Acta Crystallographica Section B*, 2006, **B62**, 1099-1111.

[11] E. Boldyreva, *Crystal Growth & Design*, 2007, **7**, 1662-1668.

[12] A. Dawson, D. R. Allan, S. A. Belmonte, S. J. Clark, W. I. F. David, P. A. McGregor, S. Parsons, C. R. Pulham and L. Sawyer, *Crystal Growth & Design*, 2005, **5**, 1415-1427.

[13] Bruker-AXS, *SAINT version 7*, Bruker-AXS, 2006

[14] G. M. Sheldrick, *SADABS Version 2008-1*, University of Gottingen, Germany and Bruker-AXS, 2008

[15] A. Altomare, G. Cascarano, C. Giacovazzo, A. Guagliardi, M. C. Burla, G. Polidori and M. Camalli, *Journal of Applied Crystallography*, 1994, **27**, 435-435.

[16] P. W. Betteridge, J. R. Carruthers, R. I. Cooper, K. Prout and D. J. Watkin, *Journal of Applied Crystallography*, 2003, **36**, 1487.

[17] Y. Sasada, T. Takano and M. Kakudo, *Bulletin of the Chemical Society of Japan*, 1964, **37**, 940-946.

[18] F. Pertlik, *Monatshefte fur Chemie*, 1990, **121**, 129-139.

[19] L. Merrill and W. A. Bassett, *Review of Scientific Instruments*, 1974, **45**, 290-294.

[20] S. A. Moggach, D. R. Allan, S. Parsons and J. E. Warren, *Journal of Applied Crystallography*, 2008, **41**, 249-251

[21] G. J. Piermarini, S. Block, J. D. Barnett and R. A. Forman, *Journal of Applied Physics*, 1975, **46**, 2774-2780.

[22] A. Dawson, D. R. Allan, S. Parsons and M. Ruf, *Journal Applied Crystallography*, 2004, **37**, 410-416.

[23] S. Parsons, *ECLIPSE*, The University of Edinburgh, 2004

[24] S. Parsons, *SHADE- Program for empirical absorption corrections to high pressure data*, University of Edinburgh, 2004

[25] R. H. Blessing, *Journal of Applied Crystallography*, 1997, **30**, 421-426.

[26] R. H. Blessing, *Crystallography Reviews*, 1987, **1**, 3-58.

[27] A. Altomare, M. C. Burla, M. Camalli, G. Cascarano, C. Giacovazzo, A. Guagliardi, A. G. G. Moliterni, G. Polidori and R. Spagna, *Journal of Applied Crystallography*, 1999, **32**, 115-119.

[28] B. Delley, *Journal of Chemical Physics*, 1990, **92**, 508-517.

[29] Accelrys, *Materials Studio Release Notes, Release 4.4* Accelrys Software Inc., 2008

[30] J. P. Perdew and Y. Wang, *Phys. Rev. B*, 1992, **45**, 13244-13249.

[31] D. Colognesi, M. Celli, F. Cilloco, R. J. Newport, S. F. Parker, V. Rossi-Albertini, F. Sacchetti, J. Tomkinson and M. Zoppi, *Applied Physics*, 2002, **A74(Suppl)**, S64-S66.

[32] A. J. Ramirez-Cuesta, *Computer Physics Communications*, 2004, **157**, 226-238.

[33] M. J. Frisch, G. W. Trucks, H. B. Schlegel, G. E. Scuseria, M. A. Robb, J. R. Cheeseman, J. J. A. Montgomery, T. Vrevren, K. N. Kudin, J. C. Burant, J. M. Millam, S. S. Iyengar, J. Tomasi, V. Barone, B. Mennucci, M. Cossi, G. Scalmani, N. Rega, G. A. Petersson, H. Nakatsuji, M. Hada, M. Ehara, K. Toyota, R. Fukuda, J. Hasegawa, M. Ishida, T. Nakajima, Y. Honda, O. Kitao, H. Nakai, M. Klene, X. Li, J. E. Knox, H. P. Hratchian, J. B. Cross, V. Bakken, C. Adamo, J. Jaramillo, R. Gomperts, R. E. Stratmann, O. Yazyev, A. J. Austin, R. Cammi, C. Pomelli, J. W. Ochterski, P. Y. Ayala, K. Morokuma, G. A. Voth, P. Salvador, J. J. Dannenberg, V. G. Zakrzewski, S. Dappricj, A. D. Daniels, M. C. Strain, O. Farkas, D. K. Malick, A. D. Rabuck, K. Raghavachari, J. B. Foresman, J. V. Oritz, Q. Cui, A. G. Baboul, S. Clifford, J. Cioslowski, B. B. Stefanov, G. Liu, A. Liashenko, P. Piskorz, I. Komaromi, R. L. Martin, D. J. Fox, T. Keith, M. A. Al-Laham, C. Y. Peng, A. Nanayakkara, M. Challacombe, P. M. W. Gill, B. Johnson, W. Chen, M. W. Wong, C. Gonzalez and J. A. Pople, *Gaussian 03 revision E.01*, 2004

[34] A. Gavezzotti, *OPIX - A computer program package for the calculation of intermolecular interactions and crystal energies*, 2003

[35] A. Gavezzotti, *Zeitschrift fuer Kristallographie*, 2005, **220**, 499-510.

[36] A. Gavezzotti, *Molecular Aggregation: Structure Analysis and Molecular Simulation of Crystals and Liquids*, Oxford University Press, Oxford,UK, 2007.

[37] J. J. McKinnon, M. A. Spackman and A. S. Mitchell, *Acta Crystallographica, Section B*, 2004, **60**, 627-668.

[38] S. K. Wolff, D. J. Grimwood, J. J. McKinnon, D. Jayatilaka and M. A. Spackman, *CrystalExplorer 2.0*, University of Western Australia, 2007

[39] D. J. Watkin, L. Pearce and K. Prout, *CAMERON - A Molecular Graphics Package*, University of Oxford, 1993

[40] C. F. Macrae, I. J. Bruno, J. A. Chisholm, P. R. Edgington, P. McCabe, E. Pidcock, L. Rodriguez-Monge, R. Taylor, J. v. d. Streek and P. A. Wood, *Journal Applied Crystallography*, 2008, **41**, 466-470.

[41] K. Brandenburg and H. Putz, *DIAMOND, version 3.2*, Crystal Impact, 2005

[42] CrystalMaker, *A crystal and molecular structures program for MAC and Windows*, CrystalMaker Software Ltd., 2009

[43] A. L. Spek, *Journal of Applied Crystallography*, 2003, **36**, 7-13.

[44] L. J. Farrugia, *Journal of Applied Crystallography*, 1999, **32**, 837-838.

[45] F. H. Allen, *Acta Crystallographica, Section B*, 2002, **58**, 380-388.

[46] S. Parsons, *STRAIN - Program for calculation of linear strain tensors* University of Edinburgh, 2003

[47] R. M. Hazen and L. W. Finger, *Comparative Crystal Chemistry: Temperature, Pressure, Composition and the Variation of Crystal Structure*, John Wiley and Sons, Chichester, New York, USA, 1982.

[48] W. H. Press, S. A. Teukolsky, W. T. Vetterling and B. P. Flannery, *Numerical Recipes in Fortran, Second Edition*, Cambridge University Press, Cambridge, England, 1992.

[49] J. D. Dunitz and A. Gavezzotti, *Angewandte Chemie, International Edition*, 2005, **44**, 1766-1787.

[50] A. Gavezzotti, *Molecular Aggregation: Structure Analysis and Molecular Simulation of Crystals and Liquids*, Oxford University Press, Oxford, UK, 2007.

[51] J. Bernstein, R. E. Davis, L. Shimoni and N.-L. Chang, *Angewandte Chemie, International Edition in English*, 1995, **34**, 1555-1573.

[52] M. A. Spackman, J. J. McKinnon and D. Jayatilaka, *CrystEngComm* 2008, **10**, 377-388.

[53] R. O. Gonçalves, P. T. C. Freire, H. N. Bordallo, J. A. Lima Jr, F. E. A. Melo, J. Mendes Filho, D. N. Argyriou and R. J. C. Lima, *Journal of Raman Spectroscopy* 2009, **40**, In press. DOI 10.1002/jrs.2209.

[54] A. M. R. Teixeira, P. T. C. Freire, A. J. D. Moreno, J. M. Sasaki, A. P. Ayala, J. Mendes Filho and F. E. A. Melo, *Solid State Communications*, 2000, **116**, 405-409.

[55] A. Maczek, *Statistical Thermodynamics*, Oxford University Press, Oxford, 2002.

[56] C. E. S. Bernades and M. E. M. Piedade, *Journal of Physical Chemistry A*, 2008, **112**, 10029-10039.

[57] M. D. M. C. R. d. Silva and N. R. M. Araujo, *Journal of Chemical Thermodynamics*, 2007, **39**, 1372-1376.

[58] P. A. Wood, J. J. McKinnon, S. Parsons, E. Pidcock and M. A. Spackman, *CrystEngComm*, 2008, **10**, 368-376.

[59] M. A. Spackman and J. J. McKinnon, *CrystEngComm*, 2002, **4**, 378-392.

[60] E. Pidcock, *Chemical Communications*, 2005, 3457-3459.

[61] C. Murli, S. M. Sharma, S. Karmakar and S. K. Sikka, *Physica B: Condensed Matter (Amsterdam, Netherlands)*, 2003, **339**, 23-30.

[62] S. A. Moggach, W. G. Marshall and S. Parsons, *Acta Crystallographica, Section B: Structural Science*, 2006, **B62**, 815-825.

[63] P. A. Wood, D. Francis, W. G. Marshall, S. A. Moggach, S. Parsons, E. Pidcock and A. L. Rohl, *CrystEngComm*, 2008, **10**, 1154 - 1166.

[64] R. D. L. Johnstone, D. Francis, A. R. Lennie, W. G. Marshall, S. A. Moggach, S. Parsons, E. Pidcock and J. E. Warren, *CrystEngComm*, 2008, **10**, 1758-1769.

[65] S. A. Rivera, D. G. Allis and B. S. Hudson, *Crystal Growth & Design*, 2008, **8**, 3905-3907.